

Verification of asymptotic homogenization method developed for periodic architected materials in strain gradient continuum

Hua Yang^a, B. Emek Abali ^{*b}, Wolfgang H. Müller ^a,
Salma Barboura^c and Jia Li^c

^a*Technische Universität Berlin, Berlin Germany*

^b*Uppsala University, Uppsala, Sweden*

^c*Sorbonne Paris North University, Paris, France*

Abstract

Strain gradient theory is an accurate model for capturing size effects and localization phenomena. However, the challenge in identification of corresponding constitutive parameters limits the practical application of such theory. We present and utilize asymptotic homogenization herein. All parameters in rank four, five, and six tensors are determined with the demonstrated computational approach. Examples for epoxy carbon fiber composite, metal matrix composite, and aluminum foam illustrate the effectiveness and versatility of the proposed method. The influences of volume fraction of matrix, the stack of RVEs, and the varying unit cell lengths on the identified parameters are investigated. The homogenization computational tool is applicable to a wide class materials and makes use of open-source codes in FEniCS.

Keywords: Strain gradient elasticity, Asymptotic homogenization method, Finite element method, constitutive parameters identification

1 Introduction

Composite materials have been widely used in engineering practice. Due to the heterogeneous nature of composites, the mechanical properties of such materials are dependent on their substructures, for example, the material properties of matrix and reinforcements, the shape of inclusions, or the volume fraction of matrix, etc. An accurate determination of effective properties of these heterogeneous media plays an important role in the design and analysis of composites. Experiments could be conceived to evaluate their effective properties, but it is also possible to compute effective material parameters by means of homogenization method [12, 42, 18, 24], which reduces the demands for experiments and enables to study microstructure of any complex geometries.

Homogenization techniques [8, 20, 72, 78, 26, 39, 46, 45] allow to represent a heterogeneous elastic material, at the microscale, as an equivalent homogeneous elastic material at the macroscale. Although of primary importance, the conventional homogenization fails to describe the mechanical responses when the heterogeneity of the material is of the same order of the macroscale. This is due to the fact that the conventional homogenization methods are based on a separation of scales, given by $\epsilon = l/L$, $l \ll L$. Here, l represents the typical length scale characteristic of the microstructural heterogeneity and L stands for the macroscopic length scale. If the microstructure consists of relatively very small heterogeneity, or the macroscopic length is infinite large, classical homogenization gives an adequate estimate of the average macroscopic properties [43, 77, 41]. However, if the size of heterogeneity is of the same order of magnitude as that of the macroscopic problem, conventional homogenization technique may fail. For example, size effects occur when the length scale of the macroscopic heterogeneous materials (L) tends to approach the length scale of the underlying heterogeneity (l). An up-scaling of Cauchy theory indicates that additional terms are necessary in the constitutive equations [55] in order to predict size effects observed in experiments [60].

*Corresponding author: bilenemek@abali.org

In order to incorporate these additional terms, different homogenization techniques are proposed in the literature, for example in the framework of generalized mechanics [57, 32, 36, 34, 7] such as micropolar theory [50, 25, 76], couple stress [71], strain gradient theory [78, 48, 40, 4, 59, 73, 36], and micromorphic continuum [67, 44]. The task of obtaining homogenized constitutive equations for generalized continua is challenging and a number of debates are active in the literature [50, 25, 54, 28, 66, 37]. Many methods have been proposed to construct strain gradient continua by means of asymptotic homogenization approaches [18, 13, 19, 76], computational approaches [49], dynamic methods [61, 70, 68], and several other identification techniques [23, 22, 58, 3, 6, 5, 65]. Asymptotic homogenization method improves descriptions by exploiting higher order terms and considering their role in macroscopic behaviors [18]. In [52, 53, 14, 74, 2], an asymptotic homogenization based solution was provided to determine parameters of composite materials. Two issues were addressed therein. One is that the identified strain gradient parameters are all zero when structures are homogeneous. The other one is that these parameters are independent of stack of RVEs. In this paper, we briefly recall the homogenization method described in [74]. The method is used to determine 2D and 3D composite materials effective parameters, including epoxy carbon fiber composite material, SiC/Al metal matrix composite, and aluminum foam.

The remainder of this paper is structured as follows: In Section 2, the underlying method is briefly explained. In Section 3, the details of numerical implementation are demonstrated. In Section 4, effective parameters for 2D and 3D composite materials including epoxy-carbon fiber composites, metal matrix composite, and aluminum foam are identified. The homogenization computational tool is developed based on open-source codes in FEniCS. It allows for all kinds of 2D or 3D composite materials constructed by periodic microstructures.

2 Homogenization method

We start from an assertion that the deformation energy for the domain representing RVE, Ω_P , at the microscale is equal to the energy for the RVE at the macroscale, namely

$$\int_{\Omega_P} w^m dV = \int_{\Omega_P} w^M dV . \quad (1)$$

The superscripts ‘‘m’’ and ‘‘M’’ are used to denote microscopic and macroscopic quantities, respectively. At the microscale, detailed microstructures are present in the RVE. At the macroscale, the same domain is modeled by a homogeneous ‘‘metamaterial’’. We emphasize that an RVE can be different from a unit cell. A unit cell is the simplest repeating unit of heterogeneity. Spatial repetition of unit cells composes RVEs. At the microscale, the first order theory is used, and at the macroscale, second order theory is employed. Now by starting with a linear strain measure, for a quadratic deformation energy we obtain

$$\int_{\Omega_P} \frac{1}{2} C_{ijkl}^m u_{i,j}^m u_{k,l}^m dV = \int_{\Omega_P} \left(\frac{1}{2} C_{ijkl}^M u_{i,j}^M u_{k,l}^M + G_{ijklm}^M u_{i,j}^M u_{k,lm}^M + \frac{1}{2} D_{ijklmn}^M u_{i,jk}^M u_{l,mn}^M \right) dV . \quad (2)$$

C_{ijkl}^m is given in each material point of the RVE. We begin with the known microscale and search for its corresponding homogenized model parameters. The effective coefficients, C_{ijkl}^M , G_{ijklm}^M , and D_{ijklmn}^M are the unknowns that we are searching for. We point out that the minor symmetries $C_{ijkl}^m = C_{jikl}^m = C_{ijlk}^m$, $C_{ijkl}^M = C_{jikl}^M = C_{ijlk}^M$, $G_{ijklm}^M = G_{jiklm}^M = G_{ijlkm}^M$, $D_{ijklmn}^M = D_{jiklmn}^M = D_{ijkmln}^M$ and major symmetries $C_{ijkl}^m = C_{klij}^m$, $C_{ijkl}^M = C_{klij}^M$, $D_{ijklmn}^M = D_{lmnijk}^M$ of the classical and strain gradient stiffness tensors. In what follows, the connections between the microscopic material parameters and macroscopic ones are established.

Let us investigate the macroscopic case for an RVE, Ω_P . Firstly, the geometric center of the RVE is defined as $\bar{\mathbf{X}} = \frac{1}{V} \int_{\Omega_P} \mathbf{X} dV$. The macroscopic energy of an RVE reads as follows (the detailed derivation can be found in [74]), as the macroscopic stiffness tensors are constant in space,

$$\begin{aligned} & \int_{\Omega_P} \left(\frac{1}{2} C_{ijkl}^M u_{i,j}^M u_{k,l}^M + G_{ijklm}^M u_{i,j}^M u_{k,lm}^M + \frac{1}{2} D_{ijklmn}^M u_{i,jk}^M u_{l,mn}^M \right) dV , \\ & = \frac{V}{2} C_{ijkl}^M \langle u_{i,j}^M \rangle \langle u_{l,m}^M \rangle + V G_{ijklm}^M \langle u_{i,j}^M \rangle \langle u_{k,lm}^M \rangle + \frac{V}{2} (C_{ijklm}^M \bar{I}_{kn} + D_{ijklmn}^M) \langle u_{i,jk}^M \rangle \langle u_{l,mn}^M \rangle , \end{aligned} \quad (3)$$

$$\bar{I}_{kn} = \frac{1}{V} \int_{\Omega_P} (X_k - \bar{X}_k)(X_n - \bar{X}_n) dV . \quad (4)$$

where

$$\langle u_{i,j}^M \rangle = u_{i,j}^M \Big|_{\bar{\mathbf{X}}} , \quad \langle u_{i,jk}^M \rangle = u_{i,jk}^M \Big|_{\bar{\mathbf{X}}} . \quad (5)$$

At the microscale, the asymptotic homogenization method is used to approximate the deformation energy for the RVE. We introduce a small parameter ϵ , which is defined as $\epsilon = \frac{l}{L}$, where l is the characteristic length of the microstructure, L is the length of the macroscopic structure as shown in Fig. 1. We remark that ϵ is the so-called homothetic ratio, which shows the scaling law for strain gradient moduli. This property will be illustrated later. A local coordinate is then introduced as

$$y_j = \frac{1}{\epsilon}(X_j - \bar{X}_j), \quad (6)$$

which is used to describe the local fluctuations caused by microscopic heterogeneity. Variable \mathbf{X} is associated with the macroscopic scale. The displacement field for the RVE at the microscale is thus approximated with regard to ϵ as

$$\mathbf{u}^m(\mathbf{X}) = \mathbf{u}^0(\mathbf{X}, \mathbf{y}) + \epsilon \mathbf{u}^1(\mathbf{X}, \mathbf{y}) + \epsilon^2 \mathbf{u}^2(\mathbf{X}, \mathbf{y}) + \dots \quad (7)$$

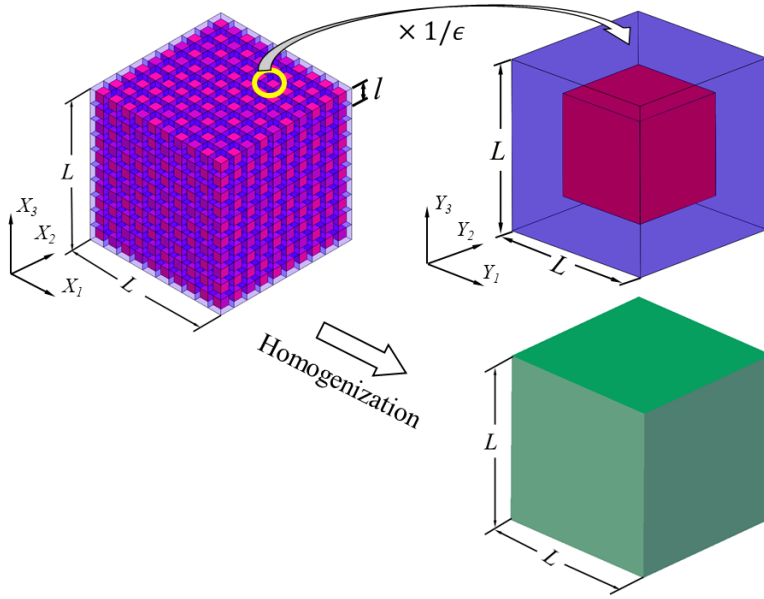


Figure 1: The heterogeneous continuum and its equivalent homogenized continuum.

For a linear elastostatics problem, the governing equation within the RVE is written as

$$(C_{ijkl}^m u_{k,l}^m)_{,j} + \rho^m f_i = 0, \quad (8)$$

where $\rho^m f_i$ are volume forces, ρ^m is the mass density at the microscale, hence it is a function in \mathbf{X} effected by the heterogeneous structure. By substituting Eqn. (7) to Eqn. (8) and gathering terms having the same order in ϵ leads to the following equations:

- in the order of ϵ^{-2}

$$\frac{\partial}{\partial y_j} \left(C_{ijkl}^m \frac{\partial u_k^0}{\partial y_l} \right) = 0; \quad (9)$$

- in the order of ϵ^{-1}

$$\left(C_{ijkl}^m \frac{\partial u_k^0}{\partial y_l} \right)_{,j} + \frac{\partial}{\partial y_j} (C_{ijkl}^m u_{k,l}^0) + \frac{\partial}{\partial y_j} \left(C_{ijkl}^m \frac{\partial u_k^1}{\partial y_l} \right) = 0; \quad (10)$$

- in the order of ϵ^0

$$\left(C_{ijkl}^m u_{k,l}^0 \right)_{,j} + \left(C_{ijkl}^m \frac{\partial u_k^1}{\partial y_l} \right)_{,j} + \frac{\partial}{\partial y_j} (C_{ijkl}^m u_{k,l}^1) + \frac{\partial}{\partial y_j} \left(C_{ijkl}^m \frac{\partial u_k^2}{\partial y_l} \right) + \rho^m f_i = 0. \quad (11)$$

The only possible solution of Eqn. (9) is to restrict $\bar{u}_i^0(\mathbf{X})$ as

$$\bar{u}_i^0 = \bar{u}_i^0(\mathbf{X}) . \quad (12)$$

Because $\bar{u}_i^0(\mathbf{X})$ is only dependent on the macroscopic coordinates, from Eqn. (7), it is obvious that it is the macroscopic displacement $\bar{u}_i^0(\mathbf{X}) = u_i^M(\mathbf{X})$. After substituting Eqn. (12) into Eqn. (10), and introducing $\varphi_{abc} = \varphi_{abc}(\mathbf{y})$ which is \mathbf{y} -periodic with zero average value $\int_{\Omega_P} \varphi_{abi} dV = 0$, we obtain

$$\frac{\partial}{\partial y_j} \left(C_{ijkl}^m \left(\frac{\partial \varphi_{abk}}{\partial y_l} + \delta_{ak} \delta_{bl} \right) \right) = 0 . \quad (13)$$

Consequently, the solution of Eqn. (10) is given as

$$\bar{u}_i^1 = \varphi_{abi} u_{a,b}^M(\mathbf{X}) + \bar{u}_i^1(\mathbf{X}) , \quad (14)$$

where $\bar{u}_i^1 = \bar{u}_i^1(\mathbf{X})$ are integration constants.

By recalling the governing equation at the macroscale, we have

$$C_{ijkl}^M u_{k,lj}^M - D_{ijklmn}^M u_{i,mnjk}^M + \rho^M f_i = 0 , \quad (15)$$

with $\rho^M = \frac{1}{V} \int_{\Omega_P} \rho^m dV$ and the assumption that f_i keeps unchanged at the micro- and macroscales. By neglecting the fourth order term in Eqn. (15), we obtain

$$f_i = - \frac{C_{ijkl}^M u_{k,lj}^M}{\rho^M} . \quad (16)$$

By plugging Eqn. (12), Eqn. (14) (with $\bar{u}_i^1(\mathbf{X}) = 0$), and Eqn. (16) into Eqn. (11) and introducing ψ_{abci} which is \mathbf{y} -periodic with zero average $\int_{\Omega_P} \psi_{abci} dV = 0$, the solution of \bar{u}_i^2 may be given as:

$$\bar{u}_i^2 = \psi_{abci} u_{a,bc}^M(\mathbf{X}) + \bar{u}_i^2(\mathbf{X}) , \quad (17)$$

where $\bar{u}_i^2(\mathbf{X})$ are integration constants in \mathbf{y} . The fourth order tensor ψ_{abcd} must satisfy

$$\frac{\partial}{\partial y_j} \left(C_{ijkl}^m \left(\frac{\partial \psi_{abck}}{\partial y_l} + \varphi_{abk} \delta_{lc} \right) \right) + C_{ickl}^m \left(\frac{\partial \varphi_{abk}}{\partial y_l} + \delta_{ka} \delta_{lb} \right) - \frac{\rho^m}{\rho^M} C_{icab}^M = 0 . \quad (18)$$

Therefore, the microscale displacement field is rewritten as

$$u_i^m(\mathbf{X}, \mathbf{y}) = u_i^M(\mathbf{X}) + \epsilon \varphi_{abi}(\mathbf{y}) u_{a,b}^M(\mathbf{X}) + \epsilon^2 \psi_{abci}(\mathbf{y}) u_{a,bc}^M(\mathbf{X}) + \dots . \quad (19)$$

By using Eqn. (19) and the latter on the left-hand side of Eqn. (2) the microscopic energy becomes

$$\int_{\Omega_P} \frac{1}{2} C_{ijkl}^m u_{i,j}^m u_{k,l}^m dV = \frac{V}{2} \left(\bar{C}_{abcd} \langle u_{a,b}^M \rangle \langle u_{c,d}^M \rangle + \bar{G}_{abcde} \langle u_{a,b}^M \rangle \langle u_{c,de}^M \rangle + \bar{D}_{abcdef} \langle u_{a,bc}^M \rangle \langle u_{d,ef}^M \rangle \right) , \quad (20)$$

with

$$\begin{aligned} \bar{C}_{abcd} &= \frac{1}{V} \int_{\Omega_P} C_{ijkl}^m L_{abij} L_{cdkl} dV , \\ \bar{G}_{abcde} &= \frac{2\epsilon}{V} \int_{\Omega_P} C_{ijkl}^m L_{abij} M_{cdekl} dV \\ \bar{D}_{abcdef} &= \frac{\epsilon^2}{V} \int_{\Omega_P} C_{ijkl}^m M_{abcij} M_{defkl} dV , \end{aligned} \quad (21)$$

The appearance of ϵ^2 is due to the fact that Eqn. (25) is expressed in the local coordinate \mathbf{y} (The fifth order

tensor \mathbf{M} is only related to \mathbf{y}).

$$\begin{aligned} L_{abij} &= \delta_{ia}\delta_{jb} + \frac{\partial\varphi_{abi}}{\partial y_j} , \\ M_{abcij} &= y_c \left(\delta_{ia}\delta_{jb} + \frac{\partial\varphi_{abi}}{\partial y_j} \right) + \left(\varphi_{abi}\delta_{jc} + \frac{\partial\psi_{abci}}{\partial y_j} \right) . \end{aligned} \quad (22)$$

Based on Eqn. (2) the effective parameters are calculated by

$$C_{abcd}^M = \frac{1}{V} \int_{\Omega_P} C_{ijkl}^m L_{abij} L_{cdkl} dV , \quad (23)$$

$$G_{abcde}^M = \frac{\epsilon}{V} \int_{\Omega_P} C_{ijkl}^m L_{abij} M_{cdekl} dV , \quad (24)$$

$$D_{abcdef}^M = \frac{\epsilon^2}{V} \left(\int_{\Omega_P} C_{ijkl}^m M_{abcij} M_{defkl} dV - C_{abde}^M \int_{\Omega_P} y_c y_f dV \right) . \quad (25)$$

It should be remarked that the Eqn. (23) coincides with the conventional asymptotic homogenization method. The classical stiffness tensor is scale independent. However, as observed from the Eqn. (25), strain gradient stiffness parameters depend on ϵ^2 . Indeed, these parameters emerge related to the substructure and vanish as $\epsilon = 0$ meaning that the substructure diminishes. We stress that this distinction is of importance and comes out of the proposed methodology quite naturally. As obvious in Eqn. (6), the homothetic ratio, ϵ , acts as a multiplier between the macroscopic length scale (in global coordinates, X) and microscopic length scale (in local coordinates, y). In this way, we acquire different \mathbf{G}^M and \mathbf{D}^M coefficients for the same RVE in larger structures. The role of ϵ will be further illustrated by using numerical examples.

3 Numerical implementation

In order to identify effective parameters, Eqn. (23) and Eqn. (25) need to be resolved, which requires φ and ψ . The tensors φ and ψ are the solutions of Eqn. (13) and Eqn. (18), which are solved numerically by the finite element method. As shown in Figure 2, six cases $\varphi_{11i}, \varphi_{22i}, \varphi_{33i}, \varphi_{23i}, \varphi_{13i}, \varphi_{12i}$ in total in 3D need to be computed under periodic boundary conditions. After using integration by parts, considering the constraints of zero average for φ , the following weak form for φ_{abk} is generated

$$\int_{\Omega^P} \left(C_{ijkl}^m \left(\frac{\partial\varphi_{abk}}{\partial y_l} + \delta_{ak}\delta_{bl} \right) \right) \frac{\partial\delta\varphi_{abi}}{\partial y_j} dV + \delta \int \lambda_{abi} \phi_{abi} dV = 0 \quad (26)$$

and then immediately we have

$$\int_{\Omega^P} \left(C_{ijkl}^m \left(\frac{\partial\varphi_{abk}}{\partial y_l} + \delta_{ak}\delta_{bl} \right) \right) \frac{\partial\delta\varphi_{abi}}{\partial y_j} dV + \int_{\Omega^P} \lambda_{abi} \delta\varphi_{abi} dV + \int_{\Omega^P} \delta\lambda_{abi} \varphi_{abi} dV = 0 , \quad (27)$$

where over underlined indices, no summation convention is applied. All fields with a variational delta, δ , denote a corresponding test function such that φ and λ are unknowns. For each case of $\varphi_{11i}, \varphi_{22i}, \varphi_{33i}, \varphi_{23i}, \varphi_{13i}, \varphi_{12i}$, a corresponding Lagrange multipliers $\lambda_{11i}, \lambda_{22i}, \lambda_{33i}, \lambda_{23i}, \lambda_{13i}, \lambda_{12i}$ are employed to enforce the zero average constrains of φ [16]. Likewise, the weak form for calculating ψ_{abci} reads

$$\begin{aligned} & \int_{\Omega^P} \left(\left(C_{ijkl}^m \left(\frac{\partial\psi_{abck}}{\partial y_l} + \varphi_{abk}\delta_{l\underline{c}} \right) \right) \frac{\partial\delta\psi_{abci}}{\partial y_j} - \right. \\ & \left. - C_{ickl}^m \left(\frac{\partial\varphi_{abk}}{\partial y_l} + \delta_{ka}\delta_{lb} \right) \delta\psi_{abci} + \frac{\rho^m}{\rho^M} C_{icab}^M \delta\psi_{abci} \right) dV + \\ & + \int_{\Omega^P} \lambda_{abci} \delta\psi_{abci} dV + \int_{\Omega^P} \delta\lambda_{abci} \psi_{abci} dV = 0 . \end{aligned} \quad (28)$$

There are 18 weak forms in 3D to be solved for $\psi_{111i}, \psi_{112i}, \dots, \psi_{123i}$.

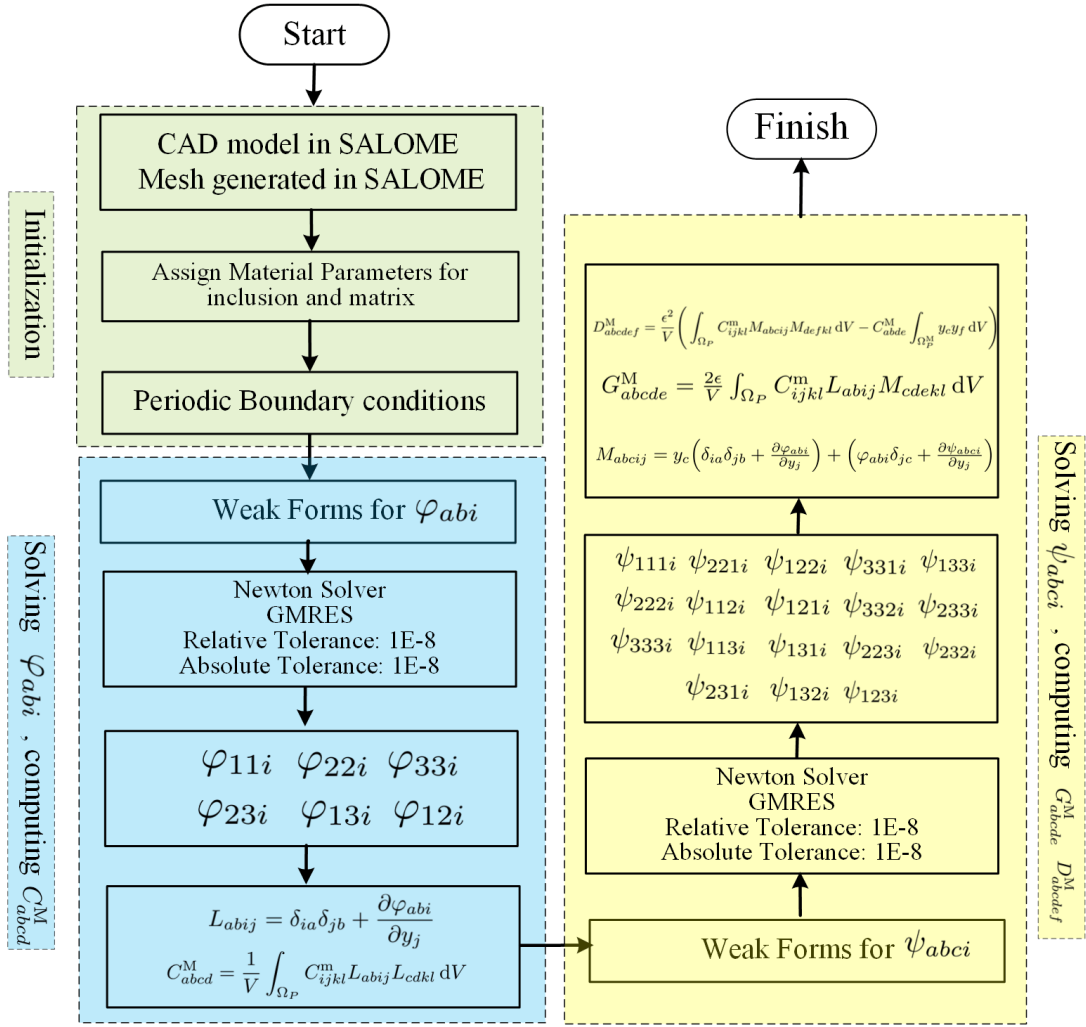


Figure 2: The flowchart of the numerical implementation.

The weak forms have been solved by the FEniCS platform. CAD model and mesh files are created by using an open-source software SALOME [1]. Triangle for surfaces elements and tetrahedron for volume elements are used to discretize the system. The same mesh is used such that the corresponding edges (in 2D) or surfaces (in 3D) are matching for nodes to be defined as the same degree of freedom in order to enforce the periodic boundary conditions as shown in Figure 3.

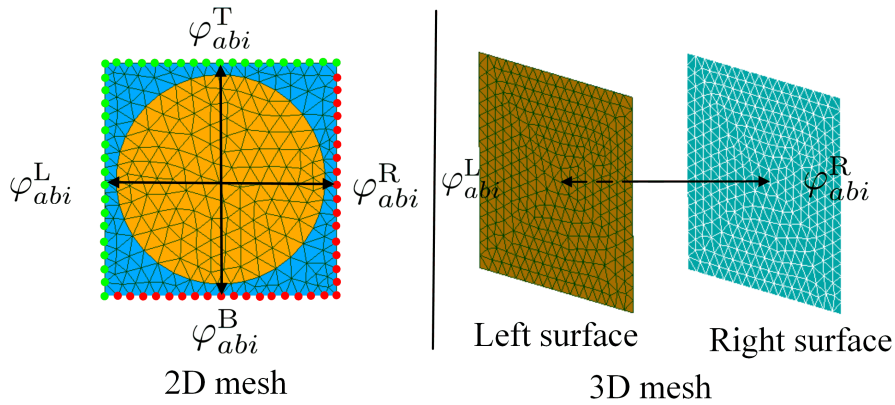


Figure 3: Periodic boundary conditions applied in FEM. Left: Right edge and green edge have the same mesh. Right: Only corresponding surfaces are shown, and so-called left surface and right surface have the same mesh. Same mesh is necessary for implementing periodic boundary conditions.

4 Numerical examples

The proposed homogenization method provides a unified analysis for general 2D and 3D composites. It can be used to homogenize fiber reinforced composites, particulate composites, and porous materials. In order to show the predictive capability of the proposed method, four examples are selected in the following.

4.1 2D epoxy-carbon fiber composite

A 2 dimensional carbon fibers reinforced epoxy composite structure is investigated. The material properties¹ for both constituents (matrix and inclusion) are shown in Table 1. The size of the unit cell is 1 mm. The fiber is of circular shape, its radius is 0.45 mm, thus, the volume fraction of matrix is 36.4%.

Table 1: Material properties used for 2D epoxy-carbon fiber composite. E Young's modulus, ν Poisson's ratio, and ρ mass density.

Type	E in GPa	ν	ρ in kg/m ³
Matrix (Epoxy)	17.3	0.35	1780
Inclusion (Carbon fiber)	35.9	0.30	1650

Voigt notations as presented in Table 2, Table 3 are used to represent rank four, five, six tensors as matrices (analogous to VOIGT's notation).

Table 2: VOIGT notation used for 2D strain tensors.

A	1	2	3
ij	11	22	12

Table 3: VOIGT notation used for 2D strain-gradient tensors.

θ	1	2	3	4	5	6
ijk	111	112	221	222	121	122

The convergence analysis is conducted as shown in Table 4. Due to the cubic material symmetry, it is expected the $C_{1111} = C_{2222}$, $D_{111111} = D_{222222}$. Therefore, when the ratios C_{1111}/C_{2222} , and D_{111111}/D_{222222} tend to be 1, the computation is converged.

Table 4: Convergence analysis. With the increasing of degrees of freedom, the ratios C_{1111}/C_{2222} , and D_{111111}/D_{222222} reach 1.

DOFs	C_{1111} GPa	C_{2222} GPa	C_{1111}/C_{2222}	D_{111111} N	D_{222222} N	D_{111111}/D_{222222}
1342	38.6	38.7	99.7 %	510.4	496.0	103.0 %
22362	38.9	38.9	100.0 %	505.3	506.1	100.0 %
90226	39.0	39.0	100.0 %	506.4	505.8	100.0 %

The solutions for φ and ψ are presented in Figure 4. It is observed that these fluctuations are all periodic. Furthermore, due to the fact that the material is cubic, rotating φ_{22} , ψ_{111} , ψ_{221} , ψ_{122} by 90 ° gives the same shapes as φ_{11} , ψ_{222} , ψ_{112} , ψ_{121} .

¹Values of material properties are taken from matweb.com

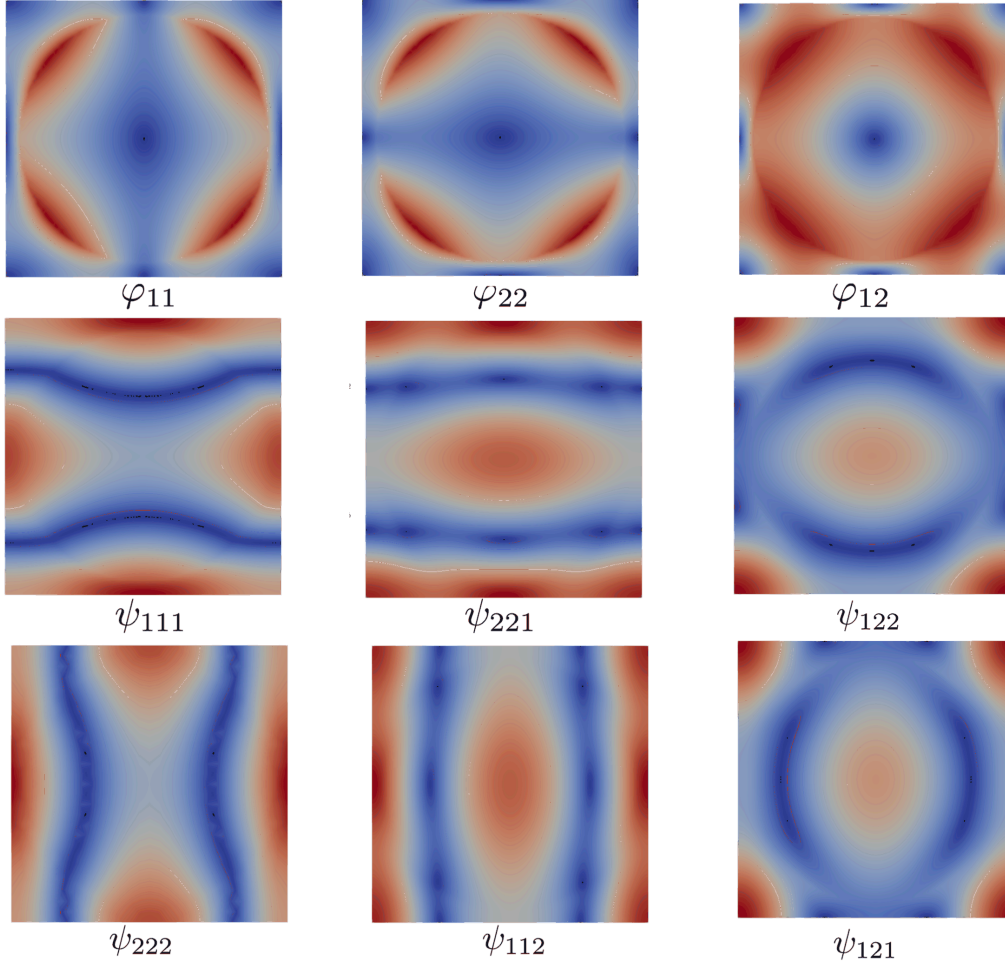


Figure 4: Solutions for φ and ψ . Color distribution showing the cubic symmetry resulted local fluctuation in φ and ψ fields. Color bars are omitted since we analyze qualitatively.

The identified effective classical and stain gradient stiffness tensors are shown as follows:

$$C_{AB}^M = \begin{pmatrix} 39.0 & 18.0 & 0.0 \\ 18.0 & 39.0 & 0.0 \\ 0.0 & 0.0 & 10.0 \end{pmatrix} \text{ GPa} ,$$

$$D_{\theta\gamma}^M = \begin{pmatrix} 506.4 & 181.9 & 0.0 & -0.0 & 0.0 & -182.2 \\ 181.9 & -299.4 & 0.0 & 0.0 & 0.0 & -176.2 \\ 0.0 & 0.0 & 181.2 & -175.4 & -183.0 & 0.0 \\ 0.0 & 0.0 & -175.4 & -298.5 & 181.2 & 0.0 \\ 0.0 & 0.0 & -183.0 & 181.2 & 505.8 & 0.0 \\ -182.2 & -176.2 & 0.0 & 0.0 & 0.0 & 181.0 \end{pmatrix} \text{ N} .$$

It is found that there are three independent parameters in the stiffness tensor and six independent parameters in the strain gradient stiffness tensor. This observation is consistent with [10, 9] for cubic materials. By using the VOIGT notation similar to the approach as in [10, 9, 11] in Table 5, the strain gradient stiffness matrix is made to be block-diagonal; each diagonal block matrix includes only non-zero parameters, and each diagonal block matrix is invariant under every cyclic permutation of \mathbf{X} axis, \mathbf{Y} axis, and \mathbf{Z} axis [11]. Therefore, the VOIGT notation proposed in [11] will be used throughout the paper.

Table 5: VOIGT notation used for 2D strain-gradient tensors proposed in [11].

α	1	2	3	4	5	6
ijk	111	221	122	222	112	121

$$D_{\alpha\beta}^M = \begin{pmatrix} 506.4 & 181.9 & -182.2 & 0.0 & 0.0 & 0.0 \\ 181.9 & -299.4 & -176.2 & 0.0 & 0.0 & 0.0 \\ -182.2 & -176.2 & 181.0 & 0.0 & 0.0 & 0.0 \\ 0.0 & 0.0 & 0.0 & 505.8 & 181.2 & -183.0 \\ 0.0 & 0.0 & 0.0 & 181.2 & -298.5 & -175.4 \\ 0.0 & 0.0 & 0.0 & -183.0 & -175.4 & 181.2 \end{pmatrix} \text{N}.$$

4.2 Interpretation of the homothetic ratio

When determining the strain gradient moduli, physical relevance of the so-called homothetic ratio, ϵ , is necessary for assessing the correct value for it. Let us consider specific cases as shown in Figure 5. In Figure 5 (a), the macroscopic length is $L = 4$ mm and the microscopic length is $l = 1$ mm. By using $\epsilon = \frac{l}{L} = \frac{1}{4}$, the 1 mm long RVE in global coordinates is magnified to 4 mm in the local coordinate. Since Eqn. (25) are expressed in the local coordinate \mathbf{y} , the parameters in D_{abcdef}^M are calculated in the local coordinate. Thus, the length of the computational domain in Eqn. (25) is 4 mm. Likewise, in Figure 5 (b), the length of integration domain is 2 times larger than that in Figure 5 (a). However $\epsilon = \frac{1}{8}$ is half of the former one. This leads to the equal values for strain gradient moduli. Consequently, in the last section, ϵ can be chosen as, for example, $\frac{1}{4}$ or $\frac{1}{8}$, as long as the corresponding length of integration domain is chosen accordingly.

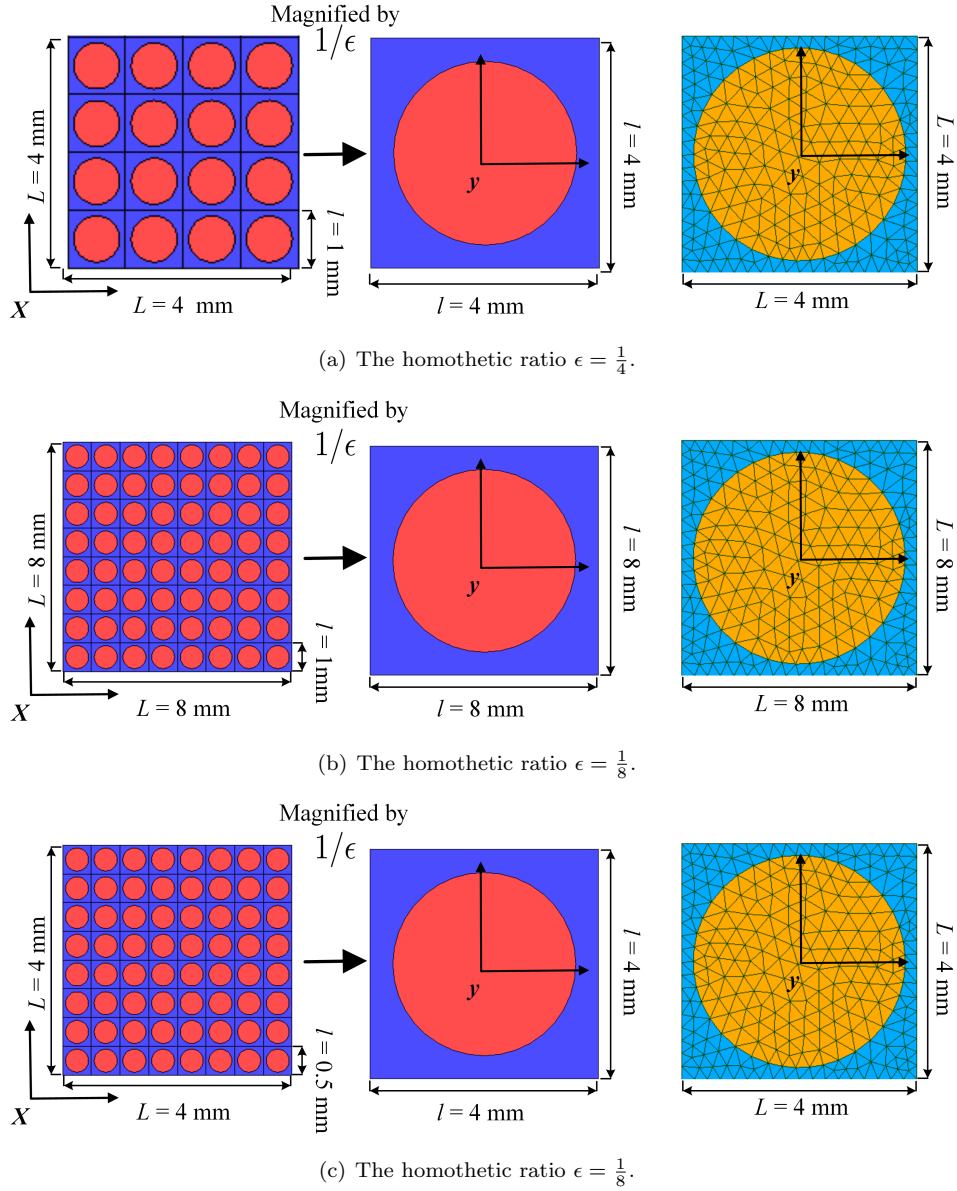


Figure 5: Visualization regarding the meaning of the homothetic ratio, ϵ , the local RVE remains the same, however, the ratio between micro- and macroscales varies.

Indeed, a scaling rule occurs for the strain gradient moduli. For example, in Figure 5 (c), the length of RVE is half of that in Figure 5 (a). The same macroscopic length equals calculated integrals in Eqn. (25). The differences of the obtained strain gradient parameters originate from the ϵ^2 as presented in Eqn. (25). The strain gradient parameters for Figure 5 (a) are 4 times larger than those for Figure 5 (c). This scaling factor is calculated as the ratio between ϵ^2 , also equal to the square of ratio of the unit cell lengths. Therefore, herein, we conclude that the strain gradient moduli is indeed not related to the macroscopic length but the microscopic length. This interpretation is indeed in coincidence with the well-known size effect in the literature. We emphasize that the substructure affects the values in C_{ijkl}^M , but not its ratio with respect to the macroscale. Therefore, for different substructures, C_{ijkl}^M needs to be recalculated. For the same substructure but different homothetic ratios, they remain the same.

4.3 3D cases

In the followings, we consider 3 dimensional cases. The effective parameters in the classical stiffness tensor and strain gradient stiffness tensor for a carbon fibers reinforced epoxy composite, a (hard) spherical particles reinforced (soft) matrix, a metal matrix composite, and an aluminum foam will be investigated. The used

VOIGT notations for these 3 dimensional cases are displayed in Table 6 and Table 7.

Table 6: VOIGT notation used for 3D strain tensors.

A	1	2	3	4	5	6
ij	11	22	33	23	13	12

Table 7: VOIGT notation used for 3D strain-gradient tensors.

α	1	2	3	4	5	6	7	8	9	10	11	12	13	14	15	16	17	18
ijk	111	221	122	331	133	222	112	121	332	233	333	113	131	223	232	231	132	123

4.3.1 3D fiber reinforced composite

Carbon fiber is modeled by using a cylinder shaped inclusion in 3D. In order to compare and validate the results, the same material properties shown in Table 1 are used for inclusion and matrix. The radius of the cylinder is of 0.45 mm so that the volume fraction of matrix reads 36.4 %, which are both equal to the example shown in 2D. The calculated parameters are shown as follows:

$$C_{AB}^M = \begin{pmatrix} 38.6 & 17.9 & 18.0 & 0.0 & 0.0 & 0.0 \\ 17.9 & 38.6 & 18.0 & 0.0 & 0.0 & 0.0 \\ 18.0 & 18.0 & 40.1 & 0.0 & 0.0 & 0.0 \\ 0.0 & 0.0 & 0.0 & 10.2 & 0.0 & 0.0 \\ 0.0 & 0.0 & 0.0 & 0.0 & 10.2 & 0.0 \\ 0.0 & 0.0 & 0.0 & 0.0 & 0.0 & 9.7 \end{pmatrix} \text{GPa} ,$$

$$D_{\alpha\beta}^M = \begin{pmatrix} 506.2 & 180.1 & -178.8 & 213.5 & 17.3 & 0.0 & 0.0 & 0.0 & 0.0 & 0.0 & 0.0 & 0.0 & 0.0 & 0.0 & 0.0 & 0.0 & 0.0 & 0.0 & 0.0 \\ 180.1 & -297.1 & -168.8 & -11.4 & -93.9 & 0.0 & 0.0 & 0.0 & 0.0 & 0.0 & 0.0 & 0.0 & 0.0 & 0.0 & 0.0 & 0.0 & 0.0 & 0.0 & 0.0 \\ -178.8 & -168.8 & 180.3 & -100.6 & -64.7 & 0.0 & 0.0 & 0.0 & 0.0 & 0.0 & 0.0 & 0.0 & 0.0 & 0.0 & 0.0 & 0.0 & 0.0 & 0.0 & 0.0 \\ 213.5 & -11.4 & -100.6 & -321.4 & -284.1 & 0.0 & 0.0 & 0.0 & 0.0 & 0.0 & 0.0 & 0.0 & 0.0 & 0.0 & 0.0 & 0.0 & 0.0 & 0.0 & 0.0 \\ 17.3 & -93.9 & -64.7 & -284.1 & 55.4 & 0.0 & 0.0 & 0.0 & 0.0 & 0.0 & 0.0 & 0.0 & 0.0 & 0.0 & 0.0 & 0.0 & 0.0 & 0.0 & 0.0 \\ 0.0 & 0.0 & 0.0 & 0.0 & 0.0 & 506.5 & 180.2 & -178.8 & 213.6 & 16.9 & 0.0 & 0.0 & 0.0 & 0.0 & 0.0 & 0.0 & 0.0 & 0.0 & 0.0 \\ 0.0 & 0.0 & 0.0 & 0.0 & 0.0 & 180.2 & -297.4 & -169.0 & -11.5 & -94.0 & 0.0 & 0.0 & 0.0 & 0.0 & 0.0 & 0.0 & 0.0 & 0.0 & 0.0 \\ 0.0 & 0.0 & 0.0 & 0.0 & 0.0 & -178.8 & -169.0 & 180.2 & -100.6 & -64.7 & 0.0 & 0.0 & 0.0 & 0.0 & 0.0 & 0.0 & 0.0 & 0.0 & 0.0 \\ 0.0 & 0.0 & 0.0 & 0.0 & 0.0 & 213.6 & -11.5 & -100.6 & -322.0 & -283.8 & 0.0 & 0.0 & 0.0 & 0.0 & 0.0 & 0.0 & 0.0 & 0.0 & 0.0 \\ 0.0 & 0.0 & 0.0 & 0.0 & 0.0 & 16.9 & -94.0 & -64.7 & -283.8 & 55.4 & 0.0 & 0.0 & 0.0 & 0.0 & 0.0 & 0.0 & 0.0 & 0.0 & 0.0 \\ 0.0 & 0.0 & 0.0 & 0.0 & 0.0 & 0.0 & 0.0 & 0.0 & 0.0 & 0.0 & 164.1 & 4.0 & -207.8 & 4.0 & -207.7 & 0.0 & 0.0 & 0.0 & 0.0 \\ 0.0 & 0.0 & 0.0 & 0.0 & 0.0 & 0.0 & 0.0 & 0.0 & 0.0 & 0.0 & 4.0 & 5.9 & 39.6 & -4.9 & -47.3 & 0.0 & 0.0 & 0.0 & 0.0 \\ 0.0 & 0.0 & 0.0 & 0.0 & 0.0 & 0.0 & 0.0 & 0.0 & 0.0 & 0.0 & -207.8 & 39.6 & 181.9 & -47.3 & -126.9 & 0.0 & 0.0 & 0.0 & 0.0 \\ 0.0 & 0.0 & 0.0 & 0.0 & 0.0 & 0.0 & 0.0 & 0.0 & 0.0 & 0.0 & 4.0 & -4.9 & -47.3 & 6.2 & 39.3 & 0.0 & 0.0 & 0.0 & 0.0 \\ 0.0 & 0.0 & 0.0 & 0.0 & 0.0 & 0.0 & 0.0 & 0.0 & 0.0 & 0.0 & -207.7 & -47.3 & -126.9 & 39.3 & 182.1 & 0.0 & 0.0 & 0.0 & 0.0 \\ 0.0 & 0.0 & 0.0 & 0.0 & 0.0 & 0.0 & 0.0 & 0.0 & 0.0 & 0.0 & 0.0 & 0.0 & 0.0 & 0.0 & 0.0 & 0.0 & -124.2 & -143.1 & -67.6 \\ 0.0 & 0.0 & 0.0 & 0.0 & 0.0 & 0.0 & 0.0 & 0.0 & 0.0 & 0.0 & 0.0 & 0.0 & 0.0 & 0.0 & 0.0 & 0.0 & -143.1 & -124.5 & -67.6 \\ 0.0 & 0.0 & 0.0 & 0.0 & 0.0 & 0.0 & 0.0 & 0.0 & 0.0 & 0.0 & 0.0 & 0.0 & 0.0 & 0.0 & 0.0 & 0.0 & -67.6 & -67.6 & 22.3 \end{pmatrix} \text{N} .$$

We stress that the algorithm computes G as well, but as expected from the centro-symmetry in the substructure, all coefficients of G vanish. The unidirectional laminate carbon reinforced epoxy composite is a transverse isotropic material. There are five independent parameters in the classical stiffness tensor, as shown below

$$C_{AB}^M = \begin{pmatrix} c_1 & c_1 - 2c_5 & c_2 & 0.0 & 0.0 & 0.0 \\ c_1 - 2c_5 & c_1 & c_2 & 0.0 & 0.0 & 0.0 \\ c_2 & c_2 & c_3 & 0.0 & 0.0 & 0.0 \\ 0.0 & 0.0 & 0.0 & c_4 & 0.0 & 0.0 \\ 0.0 & 0.0 & 0.0 & 0.0 & c_4 & 0.0 \\ 0.0 & 0.0 & 0.0 & 0.0 & 0.0 & c_5 \end{pmatrix} .$$

We stress that the computed parameters are matching this relation within a tolerance of $\pm 6.7\%$. After investigating the strain gradient stiffness tensor, we find the relations between higher order parameters as shown in Figure 6.

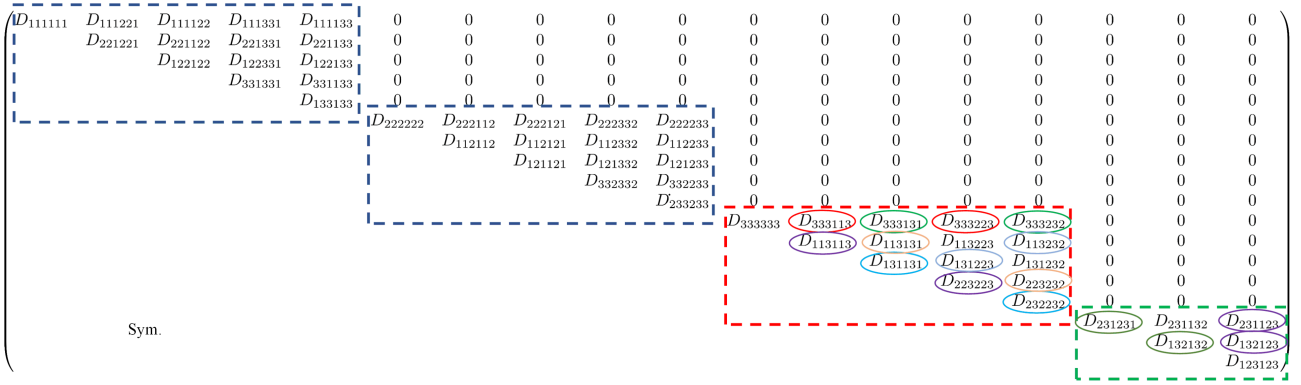


Figure 6: The structure of strain gradient stiffness tensor for transverse isotropic materials. It is found that the first two 5×5 matrices in the diagonal are equal, for example, $D_{111111} = D_{222222}$. In the third 5×5 matrix in the diagonal, it is also observed that $D_{333113} = D_{333223}$, $D_{333131} = D_{333232}$, $D_{113113} = D_{223223}$, $D_{113131} = D_{223232}$, $D_{113223} = D_{131223}$, $D_{131131} = D_{232232}$. In the 3×3 matrix, $D_{231231} = D_{132132}$, $D_{231123} = D_{132123}$.

Excluding the parameters of the same value, there are 28 parameters in \mathbf{D} for this transverse isotropic material

$$D_{\alpha\beta}^M = \begin{pmatrix} d_1 & d_2 & d_3 & d_4 & d_5 & 0 & 0 & 0 & 0 & 0 & 0 & 0 & 0 & 0 & 0 & 0 \\ & d_6 & d_7 & d_8 & d_9 & 0 & 0 & 0 & 0 & 0 & 0 & 0 & 0 & 0 & 0 & 0 \\ & & d_{10} & d_{11} & d_{12} & 0 & 0 & 0 & 0 & 0 & 0 & 0 & 0 & 0 & 0 & 0 \\ & & & d_{13} & d_{14} & 0 & 0 & 0 & 0 & 0 & 0 & 0 & 0 & 0 & 0 & 0 \\ & & & & d_{15} & 0 & 0 & 0 & 0 & 0 & 0 & 0 & 0 & 0 & 0 & 0 \\ & & & & & d_1 & d_2 & d_3 & d_4 & d_5 & 0 & 0 & 0 & 0 & 0 & 0 \\ & & & & & & d_6 & d_7 & d_8 & d_9 & 0 & 0 & 0 & 0 & 0 & 0 \\ & & & & & & & d_{10} & d_{11} & d_{12} & 0 & 0 & 0 & 0 & 0 & 0 \\ & & & & & & & & d_{13} & d_{14} & 0 & 0 & 0 & 0 & 0 & 0 \\ & & & & & & & & & d_{15} & 0 & 0 & 0 & 0 & 0 & 0 \\ & & & & & & & & & & d_{16} & d_{17} & d_{18} & d_{17} & d_{18} & 0 & 0 & 0 \\ & & & & & & & & & & & d_{19} & d_{20} & d_{21} & d_{22} & 0 & 0 & 0 \\ & & & & & & & & & & & & d_{23} & d_{22} & d_{24} & 0 & 0 & 0 \\ & & & & & & & & & & & & & d_{19} & d_{20} & 0 & 0 & 0 \\ & & & & & & & & & & & & & & d_{23} & 0 & 0 & 0 \\ & & & & & & & & & & & & & & & d_{25} & d_{27} & d_{28} \\ & & & & & & & & & & & & & & & & d_{25} & d_{28} \\ & & & & & & & & & & & & & & & & & d_{26} \end{pmatrix}.$$

We emphasize that some of the 28 parameters could be linearly dependent which leads to a reduction of independent coefficients. Moreover, the corresponding parameters in 2D and 3D stiffness tensors are equal within a tolerance of $\pm 4.4\%$, for example, C_{1111} or D_{111111} in the 2D stiffness tensors are equal to those in the 3D tensors. This verifies the calculated results. In order to further test the homogenization method, computations for different volume fraction of matrix are conducted as presented in Figure 7.

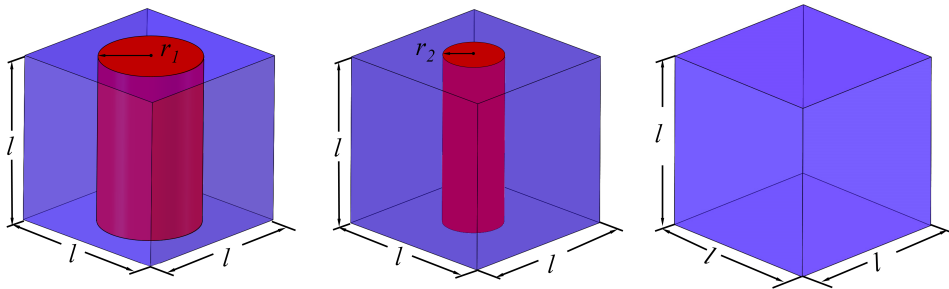


Figure 7: Different volume fraction of matrix. $l = 1$ mm, $r_1 = 0.45$ mm, $r_2 = 0.35$ mm.

The results are shown in Figure 8. It is observed that with the increasing of the volume fraction of matrix,

absolute values of most of effective parameters decrease. This is due to the fact that matrix (epoxy) is softer than inclusion (carbon). It should be emphasized that when the volume fraction of matrix is 1, namely the material is purely homogeneous, the higher order parameters vanish as expected.

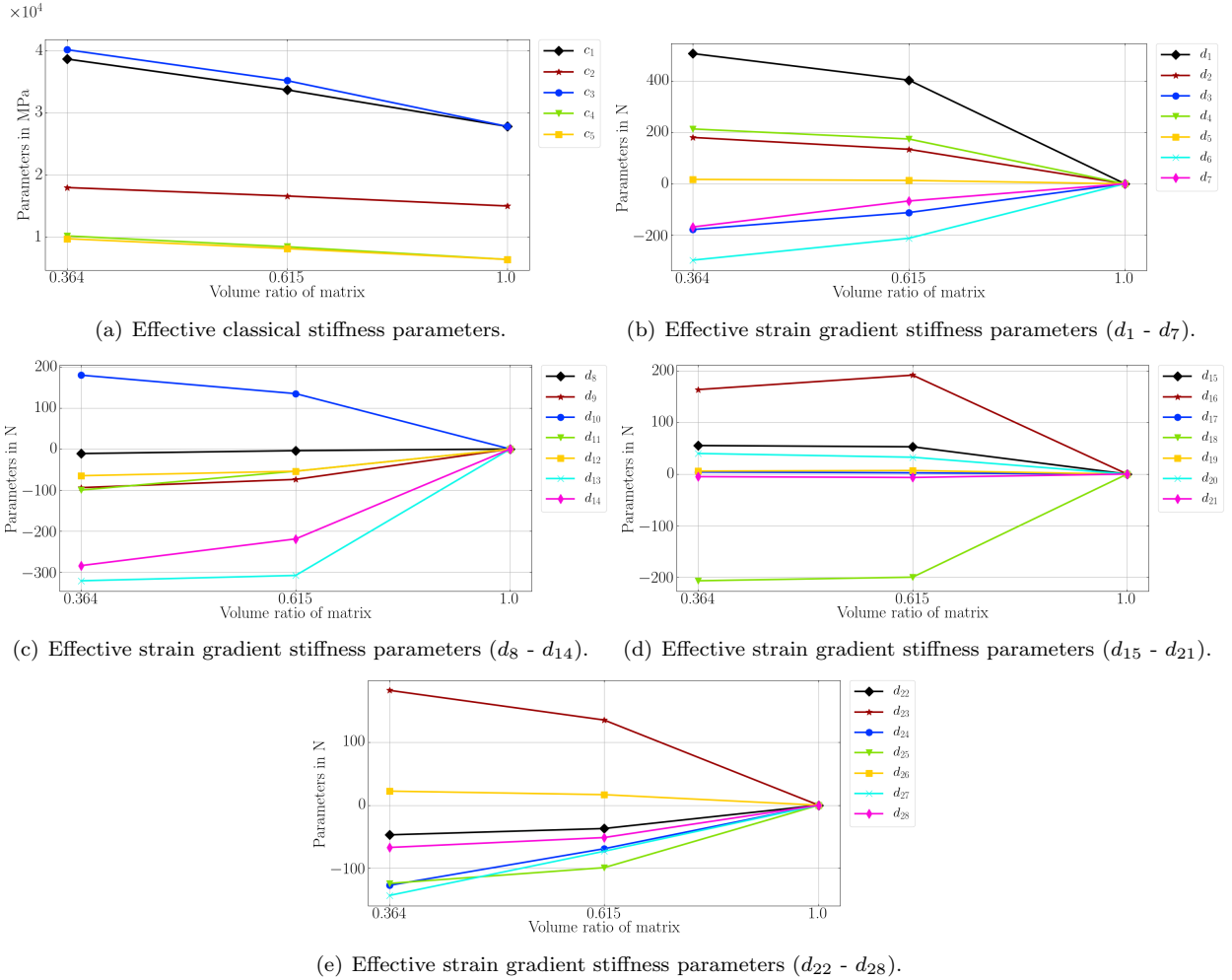


Figure 8: Effective material parameters with the changing of volume fraction of matrix. It should be noted that when the material is purely homogeneous (volume fraction of matrix is 1), all higher order parameters vanish.

Further investigations are carried out for RVEs by varying their sizes ($1\text{ mm} \times 1\text{ mm} \times 1\text{ mm}$, $2\text{ mm} \times 2\text{ mm} \times 2\text{ mm}$, $3\text{ mm} \times 3\text{ mm} \times 3\text{ mm}$) as shown in Figure 9 and Figure 10. It is found that all coefficients remain constant, which indicates that the obtained parameters are independent of the repetition of RVEs.

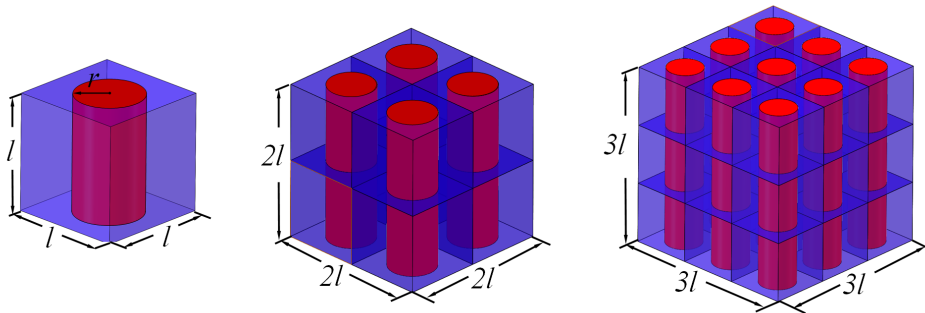


Figure 9: RVEs constructed by 1 unit cell, 8 unit cells, 27 unit cells. $l = 1\text{ mm}$, the radius of fiber is 0.45 mm .

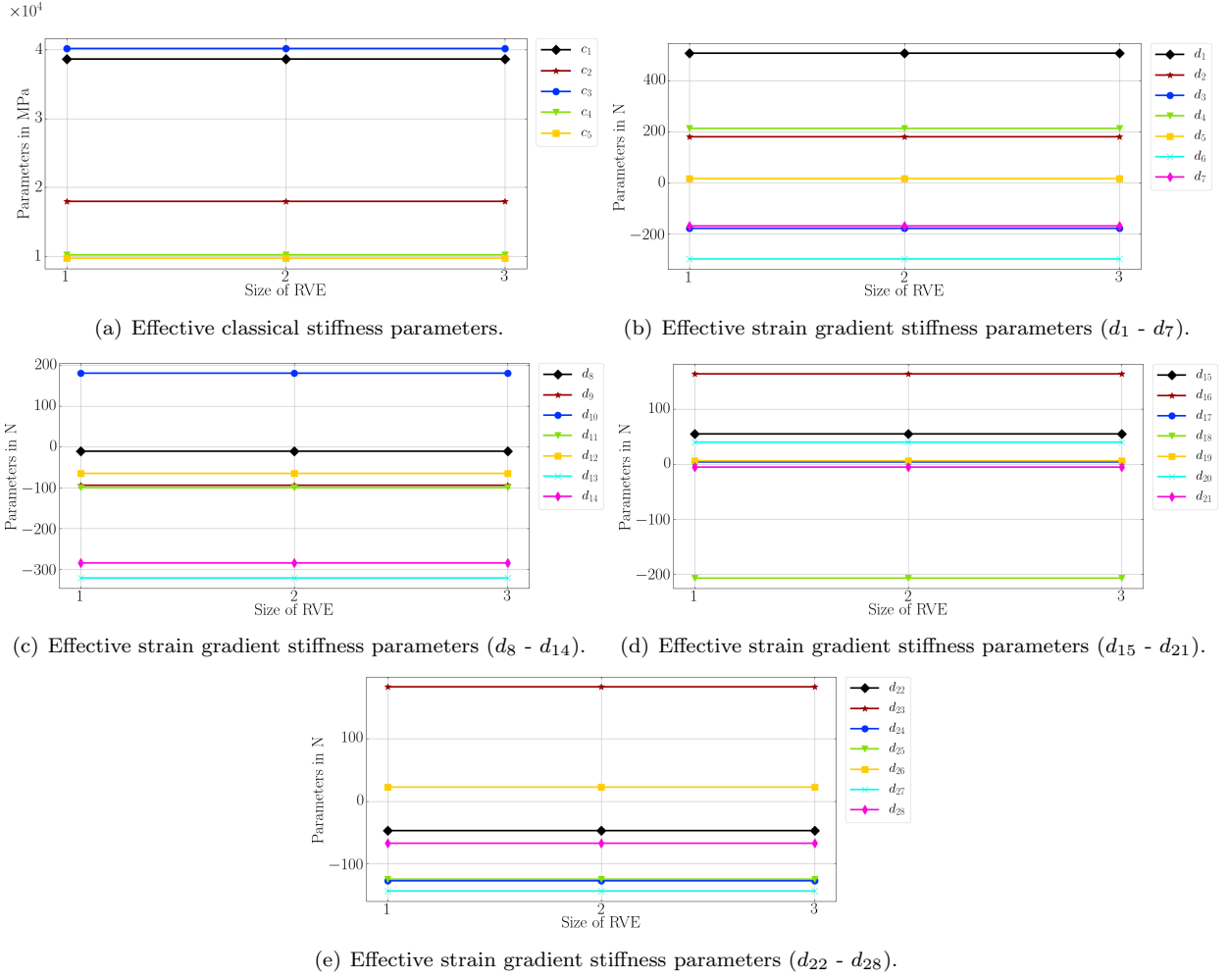


Figure 10: Effective material parameters with the repetition of RVEs (1 mm \times 1 mm \times 1 mm, 2 mm \times 2 mm \times 2 mm, 3 mm \times 3 mm \times 3 mm).

Effective parameters are studied for unit cells with varying sizes as displayed in Figure 11. The smaller unit cells are generated by homothetically scaling the larger one. Therefore, the volume fraction of matrix are identical in these cases. It is found in Figure 12 that the parameters in the classical stiffness tensor remain the same, but the ones in the strain gradient stiffness tensor vary with the changing of the unit cell lengths. This fact is because of C_{ijkl}^M being invariant regarding the microstructural size. However the effective strain gradient ones are sensitive to the homothetic ratio ϵ . These higher order parameters follow a scaling rule. For example, the parameters can be obtained for the unit cell size of 0.5 mm \times 0.5 mm \times 0.5 mm by multiplying a scaling factor with the effective parameters of the unit cell size of 1 mm \times 1 mm \times 1 mm. The scaling factor is the square of homothetic ratio ϵ^2 which is numerically equal to the square of ratio of the unit cell lengths herein.

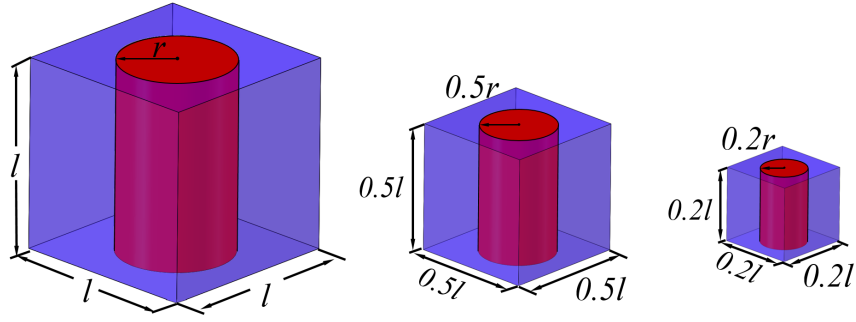


Figure 11: Unit cells with the changing sizes. $l = 1$ mm The volume fraction of matrix are kept equal.

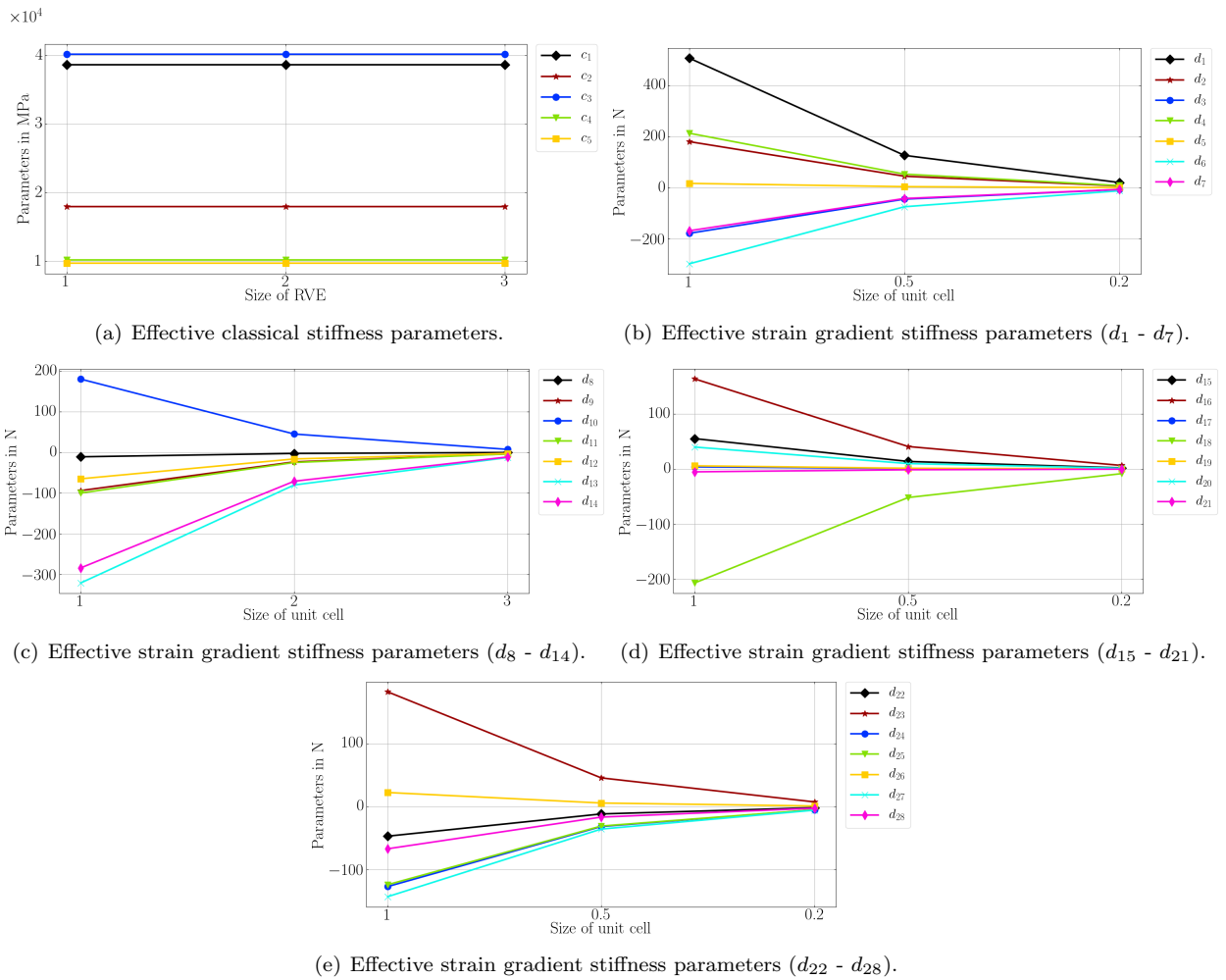


Figure 12: Effective material parameters with the changing lengths of unit cells, we emphasize that the sub-structure remains the same.

4.3.2 SiC/Al Metal Matrix Composite (MMC)

Aluminum-based MMCs have gained interest in engineering over the past few decades. The insertion of a ceramic material into a aluminum matrix leads to an fascinating mechanical properties. In this section, the effective properties of SiC/Al metal matrix composite are investigated. RVE models have been created for three-dimensional spherical particles embedded into the metal matrix. Filler is used as a reinforcement. Their volume ratios within the MMC vary from 0% to 38.2 % by volume. The material parameters taken from [17] are compiled in Table 8.

strain gradient stiffness tensor,

$$D_{\alpha\beta}^M = \begin{pmatrix} d_1 & d_2 & d_3 & d_2 & d_3 & 0 & 0 & 0 & 0 & 0 & 0 & 0 & 0 & 0 & 0 & 0 & 0 & 0 \\ & d_4 & d_5 & d_6 & d_7 & 0 & 0 & 0 & 0 & 0 & 0 & 0 & 0 & 0 & 0 & 0 & 0 & 0 \\ & & d_8 & d_7 & d_9 & 0 & 0 & 0 & 0 & 0 & 0 & 0 & 0 & 0 & 0 & 0 & 0 & 0 \\ & & & d_4 & d_5 & 0 & 0 & 0 & 0 & 0 & 0 & 0 & 0 & 0 & 0 & 0 & 0 & 0 \\ & & & & d_8 & 0 & 0 & 0 & 0 & 0 & 0 & 0 & 0 & 0 & 0 & 0 & 0 & 0 \\ & & & & & d_1 & d_2 & d_3 & d_2 & d_3 & 0 & 0 & 0 & 0 & 0 & 0 & 0 & 0 \\ & & & & & & d_4 & d_5 & d_6 & d_7 & 0 & 0 & 0 & 0 & 0 & 0 & 0 & 0 \\ & & & & & & & d_8 & d_7 & d_9 & 0 & 0 & 0 & 0 & 0 & 0 & 0 & 0 \\ & & & & & & & & d_4 & d_5 & 0 & 0 & 0 & 0 & 0 & 0 & 0 & 0 \\ & & & & & & & & & d_8 & 0 & 0 & 0 & 0 & 0 & 0 & 0 & 0 \\ & & & & & & & & & & d_1 & d_2 & d_3 & d_2 & d_3 & 0 & 0 & 0 \\ & & & & & & & & & & & d_4 & d_5 & d_6 & d_7 & 0 & 0 & 0 \\ & & & & & & & & & & & & d_8 & d_7 & d_9 & 0 & 0 & 0 \\ & & & & & & & & & & & & & d_4 & d_5 & 0 & 0 & 0 \\ & & & & & & & & & & & & & & d_8 & 0 & 0 & 0 \\ & & & & & & & & & & & & & & & d_{10} & d_{11} & d_{11} \\ & & & & & & & & & & & & & & & & d_{10} & d_{11} \\ & & & & & & & & & & & & & & & & & d_{10} \end{pmatrix}.$$

Sym.

Please note, among these 11 parameters, some of them might be linearly dependent. Further investigations are conducted for different volume fraction of matrix, different sizes of selected RVE, and different sizes of unit cells as indicated in Figures 14, 16, 18. Results are displayed in Figures 15, 17, 19. It is observed that the higher order parameters are zero when materials are homogeneous; they are independent of the stack of RVEs, and they are sensitive to microstructural sizes as well as following the scaling rule.

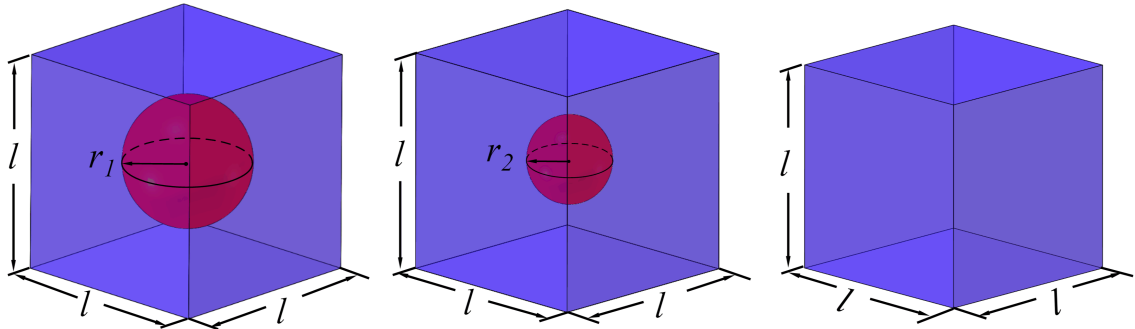


Figure 14: Changing volume fraction of matrix.

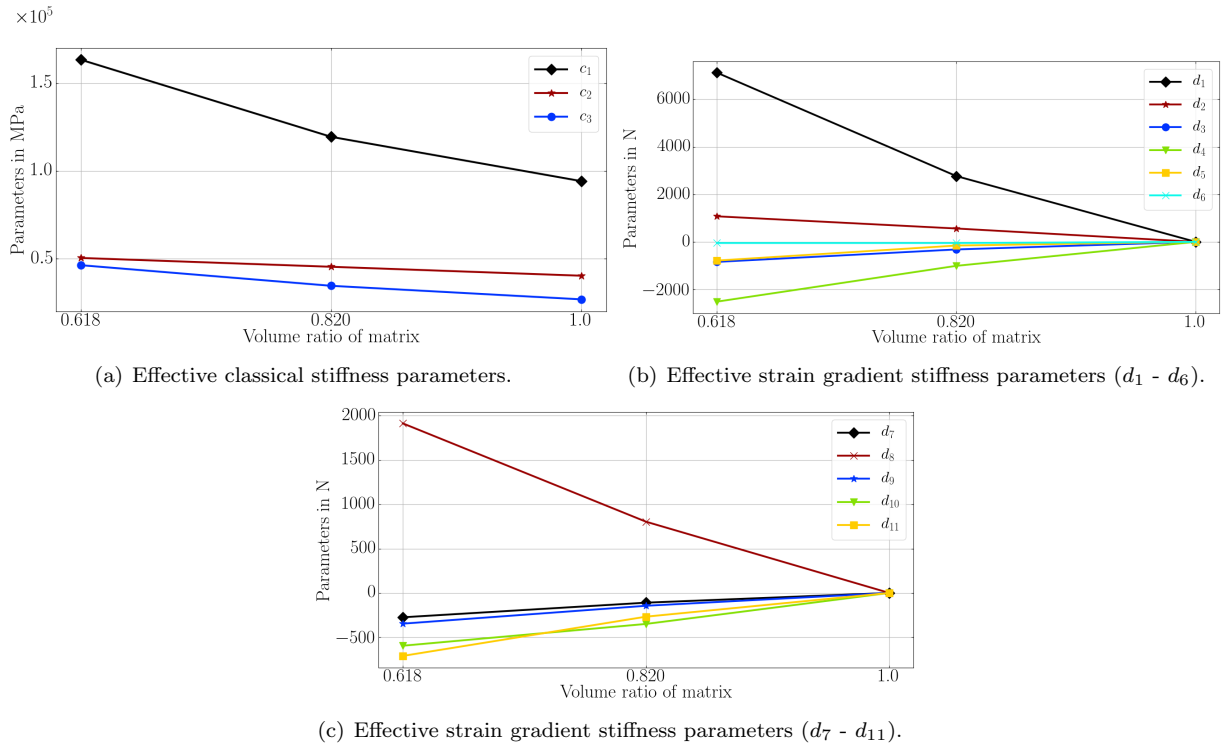


Figure 15: Effective material parameters with the changing of volume fraction of matrix.

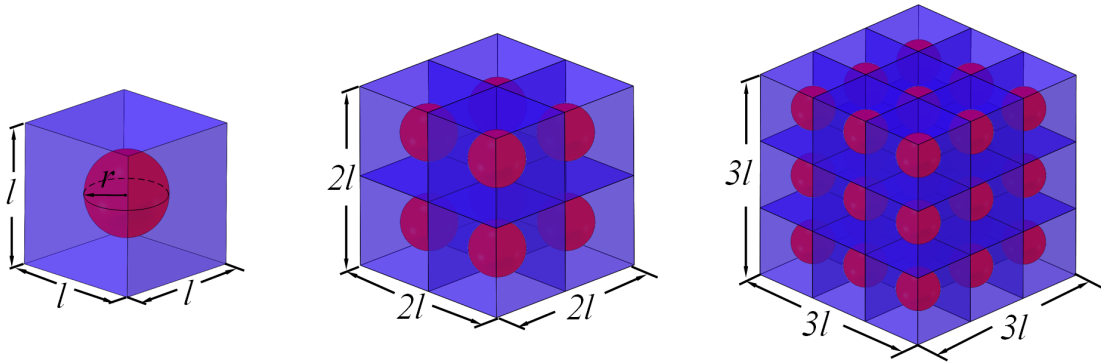


Figure 16: RVEs constructed by 1 unit cell, 8 unit cells, 27 unit cells.

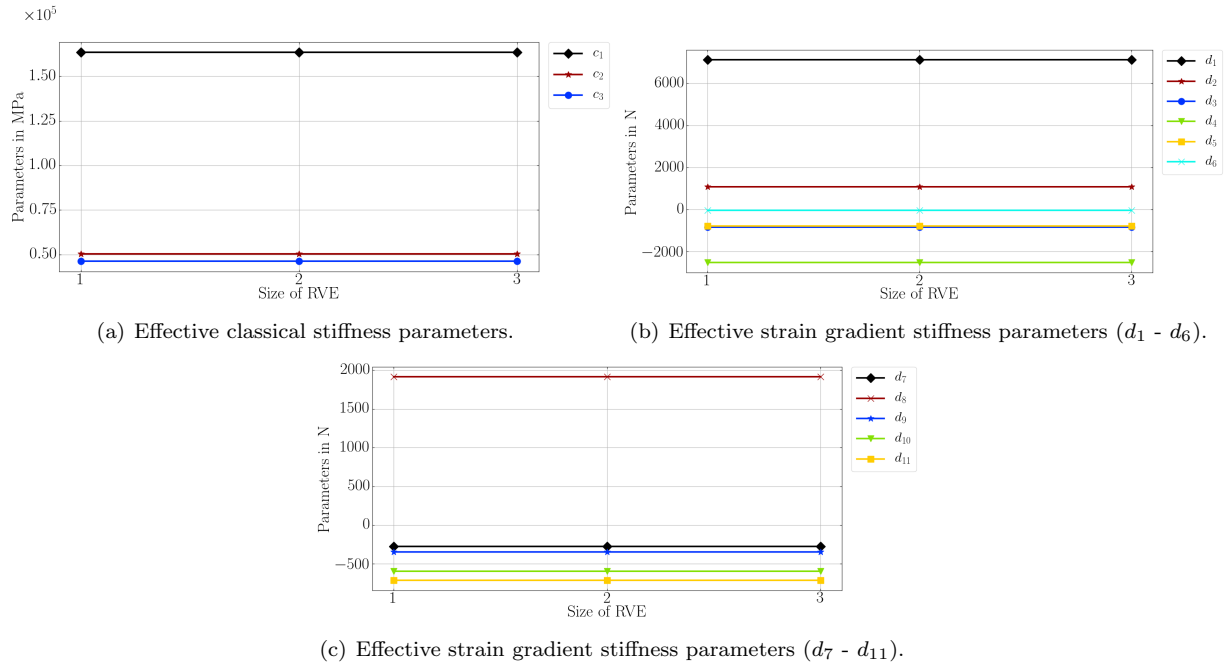


Figure 17: Effective material parameters with the changing RVE sizes ($1 \times 1 \times 1$, $2 \times 2 \times 2$, $3 \times 3 \times 3$).

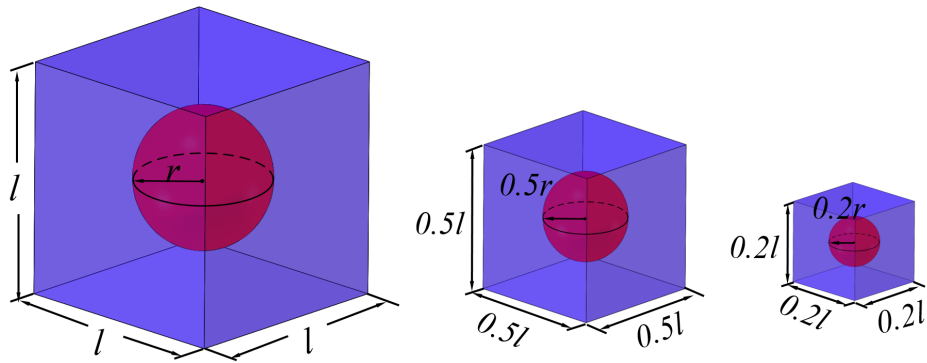


Figure 18: Unit cells with changing lengths.

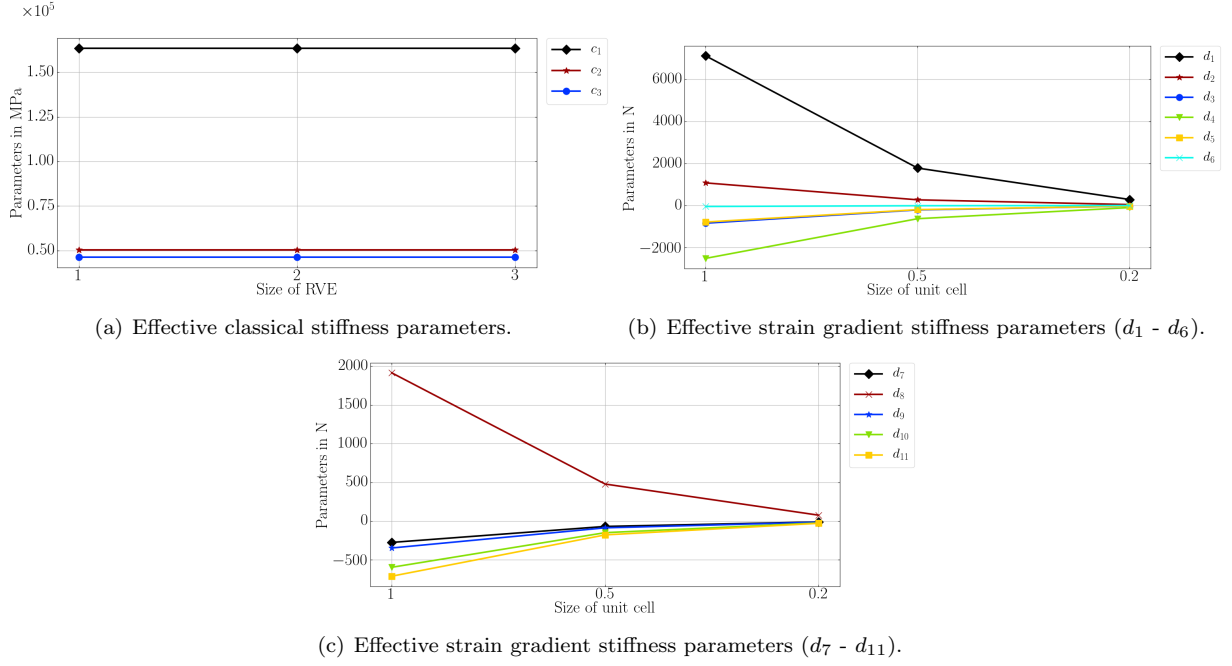


Figure 19: Effective material parameters with the changing lengths of unit cells.

4.3.3 Aluminum foam

Aluminum foam is a highly porous metallic material with a cellular substructure. The RVEs of the aluminum foam are modeled by using a cubic inclusion which are technically voids embedded in a matrix made of aluminum. In order to avoid numerical problems, a small number is assigned to the Young's modulus of voids. The material properties used for aluminum foam is found in Table 9.

Table 9: Material properties used for aluminum foam. E Young's modulus, ν Poisson's ratio, and ρ mass density.

Type	E in GPa	ν	ρ in kg/m ³
Matrix (Aluminum)	70	0.3	2700
Inclusion (Voids)	1e-10	0.0	0.0

The identified parameters are found as follows:

$$C_{AB}^M = \begin{pmatrix} 15.1 & 3.0 & 3.0 & 0.0 & 0.0 & 0.0 \\ 3.0 & 15.1 & 3.0 & 0.0 & 0.0 & 0.0 \\ 3.0 & 3.0 & 15.1 & 0.0 & 0.0 & 0.0 \\ 0.0 & 0.0 & 0.0 & 2.9 & 0.0 & 0.0 \\ 0.0 & 0.0 & 0.0 & 0.0 & 2.9 & 0.0 \\ 0.0 & 0.0 & 0.0 & 0.0 & 0.0 & 2.9 \end{pmatrix} \text{ GPa} ,$$

$$D_{\alpha\beta}^M = \begin{pmatrix} 1130.3 & 185.4 & 288.8 & 184.8 & 288.6 & 0.0 & 0.0 & 0.0 & 0.0 & 0.0 & 0.0 & 0.0 & 0.0 & 0.0 & 0.0 & 0.0 & 0.0 & 0.0 \\ 185.4 & 1080.6 & 114.9 & 328.0 & 74.6 & 0.0 & 0.0 & 0.0 & 0.0 & 0.0 & 0.0 & 0.0 & 0.0 & 0.0 & 0.0 & 0.0 & 0.0 & 0.0 \\ 288.8 & 114.9 & -42.8 & 74.5 & 160.7 & 0.0 & 0.0 & 0.0 & 0.0 & 0.0 & 0.0 & 0.0 & 0.0 & 0.0 & 0.0 & 0.0 & 0.0 & 0.0 \\ 184.8 & 328.0 & 74.5 & 1080.3 & 114.9 & 0.0 & 0.0 & 0.0 & 0.0 & 0.0 & 0.0 & 0.0 & 0.0 & 0.0 & 0.0 & 0.0 & 0.0 & 0.0 \\ 288.6 & 74.6 & 160.7 & 114.9 & -42.6 & 0.0 & 0.0 & 0.0 & 0.0 & 0.0 & 0.0 & 0.0 & 0.0 & 0.0 & 0.0 & 0.0 & 0.0 & 0.0 \\ 0.0 & 0.0 & 0.0 & 0.0 & 0.0 & 1139.1 & 187.6 & 290.6 & 186.9 & 290.2 & 0.0 & 0.0 & 0.0 & 0.0 & 0.0 & 0.0 & 0.0 & 0.0 \\ 0.0 & 0.0 & 0.0 & 0.0 & 0.0 & 187.6 & 1081.0 & 114.7 & 328.4 & 75.0 & 0.0 & 0.0 & 0.0 & 0.0 & 0.0 & 0.0 & 0.0 & 0.0 \\ 0.0 & 0.0 & 0.0 & 0.0 & 0.0 & 290.6 & 114.7 & -42.8 & 74.9 & 161.0 & 0.0 & 0.0 & 0.0 & 0.0 & 0.0 & 0.0 & 0.0 & 0.0 \\ 0.0 & 0.0 & 0.0 & 0.0 & 0.0 & 186.9 & 328.4 & 74.9 & 1080.4 & 115.4 & 0.0 & 0.0 & 0.0 & 0.0 & 0.0 & 0.0 & 0.0 & 0.0 \\ 0.0 & 0.0 & 0.0 & 0.0 & 0.0 & 290.2 & 75.0 & 161.0 & 115.4 & -42.5 & 0.0 & 0.0 & 0.0 & 0.0 & 0.0 & 0.0 & 0.0 & 0.0 \\ 0.0 & 0.0 & 0.0 & 0.0 & 0.0 & 0.0 & 0.0 & 0.0 & 0.0 & 1171.8 & 194.3 & 296.5 & 194.5 & 296.9 & 0.0 & 0.0 & 0.0 & 0.0 \\ 0.0 & 0.0 & 0.0 & 0.0 & 0.0 & 0.0 & 0.0 & 0.0 & 0.0 & 194.3 & 1082.3 & 115.6 & 329.8 & 76.3 & 0.0 & 0.0 & 0.0 & 0.0 \\ 0.0 & 0.0 & 0.0 & 0.0 & 0.0 & 0.0 & 0.0 & 0.0 & 0.0 & 296.5 & 115.6 & -42.1 & 76.3 & 162.0 & 0.0 & 0.0 & 0.0 & 0.0 \\ 0.0 & 0.0 & 0.0 & 0.0 & 0.0 & 0.0 & 0.0 & 0.0 & 0.0 & 194.5 & 329.8 & 76.3 & 1082.1 & 115.8 & 0.0 & 0.0 & 0.0 & 0.0 \\ 0.0 & 0.0 & 0.0 & 0.0 & 0.0 & 0.0 & 0.0 & 0.0 & 0.0 & 296.9 & 76.3 & 162.0 & 115.8 & -42.0 & 0.0 & 0.0 & 0.0 & 0.0 \\ 0.0 & 0.0 & 0.0 & 0.0 & 0.0 & 0.0 & 0.0 & 0.0 & 0.0 & 0.0 & 0.0 & 0.0 & 0.0 & 0.0 & 406.8 & 19.6 & 19.9 & 0.0 \\ 0.0 & 0.0 & 0.0 & 0.0 & 0.0 & 0.0 & 0.0 & 0.0 & 0.0 & 0.0 & 0.0 & 0.0 & 0.0 & 0.0 & 19.6 & 406.7 & 19.8 & 0.0 \\ 0.0 & 0.0 & 0.0 & 0.0 & 0.0 & 0.0 & 0.0 & 0.0 & 0.0 & 0.0 & 0.0 & 0.0 & 0.0 & 0.0 & 19.9 & 19.8 & 406.9 & 0.0 \end{pmatrix} \text{N}.$$

Three independent parameters and eleven parameters are observed in the classical stiffness tensor and the strain gradient stiffness tensor, respectively. This is consistent to the cubic material symmetry as mentioned before. Investigations on the different volume fraction of matrix, repetition of RVEs, changing sizes of unit cells are conducted as displayed in Figures 20, 22, 24. Corresponding outcomes are presented in Figures 21, 23, 25.

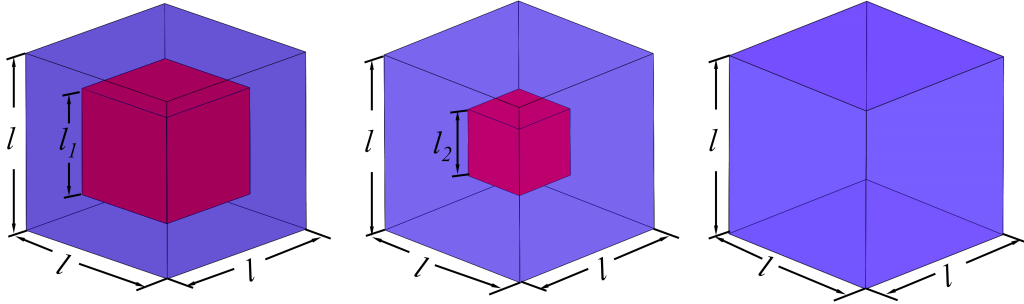


Figure 20: Different volume fraction of matrix for the aluminum foam.

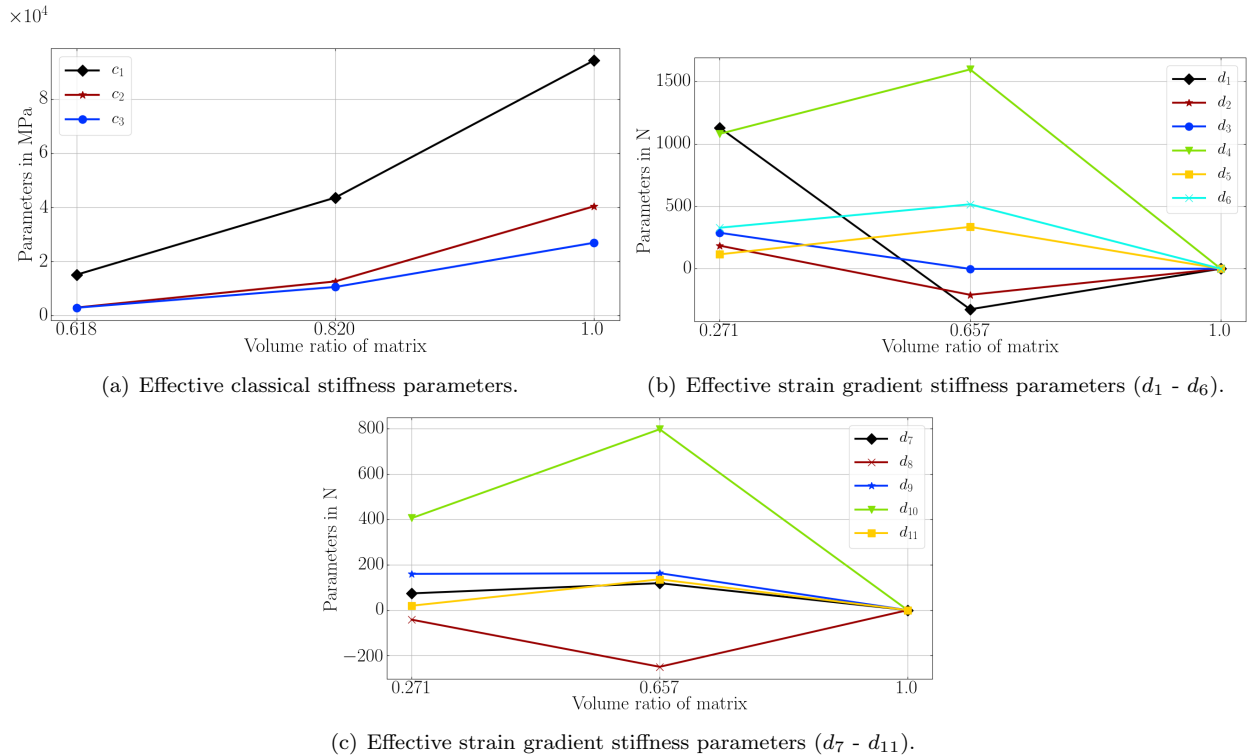


Figure 21: Effective material parameters with changing of volume fraction of matrix.

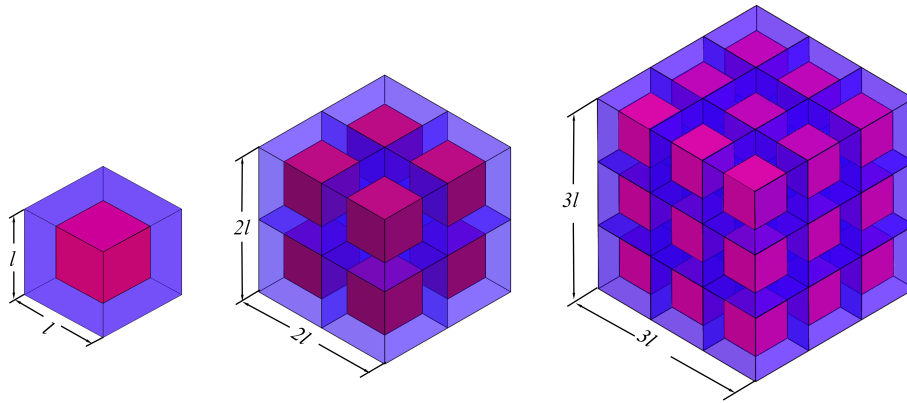


Figure 22: RVEs constructed by 1 unit cell, 8 unit cells, 27 unit cells.

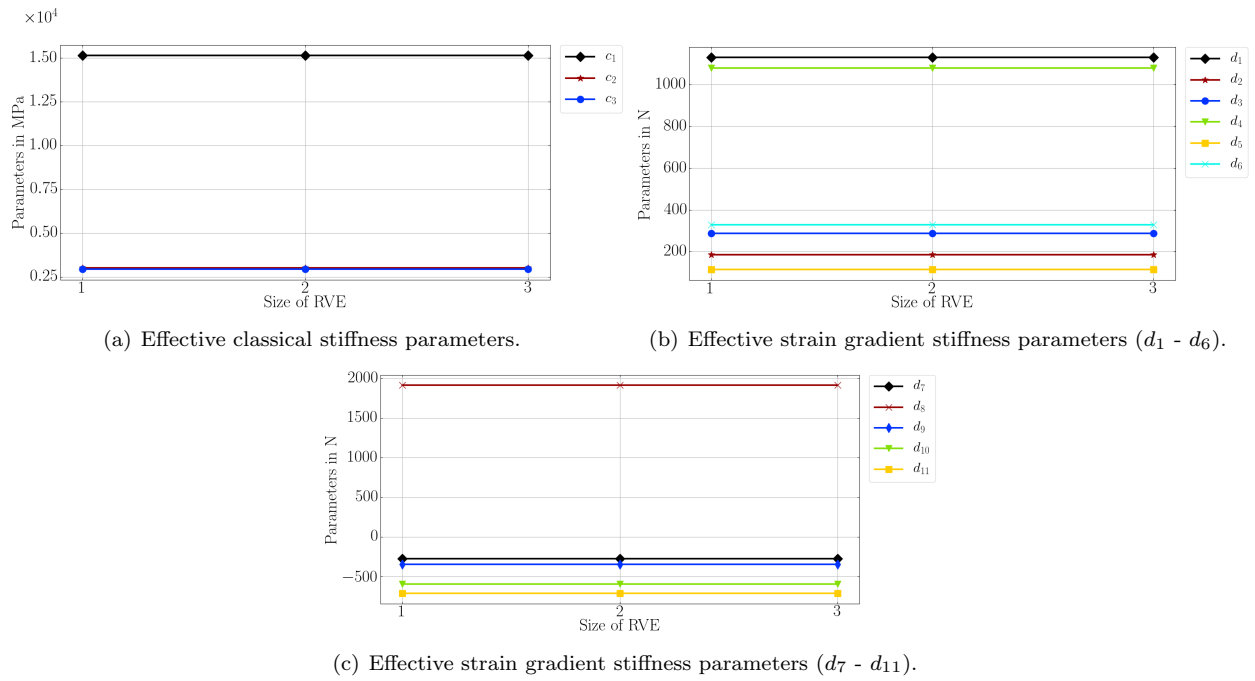


Figure 23: Effective material parameters with changing RVE sizes ($1 \times 1 \times 1$, $2 \times 2 \times 2$, $3 \times 3 \times 3$).

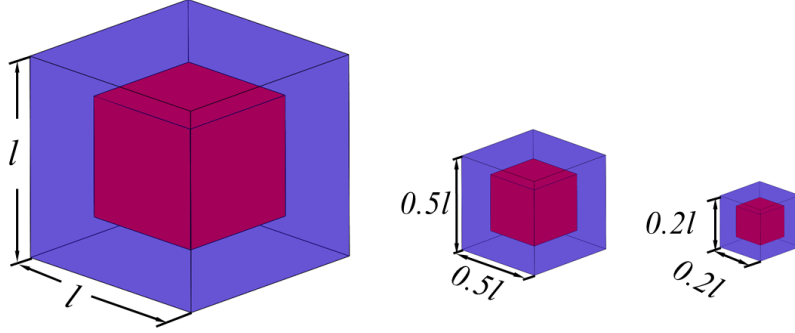


Figure 24: Unit cells with changing lengths.

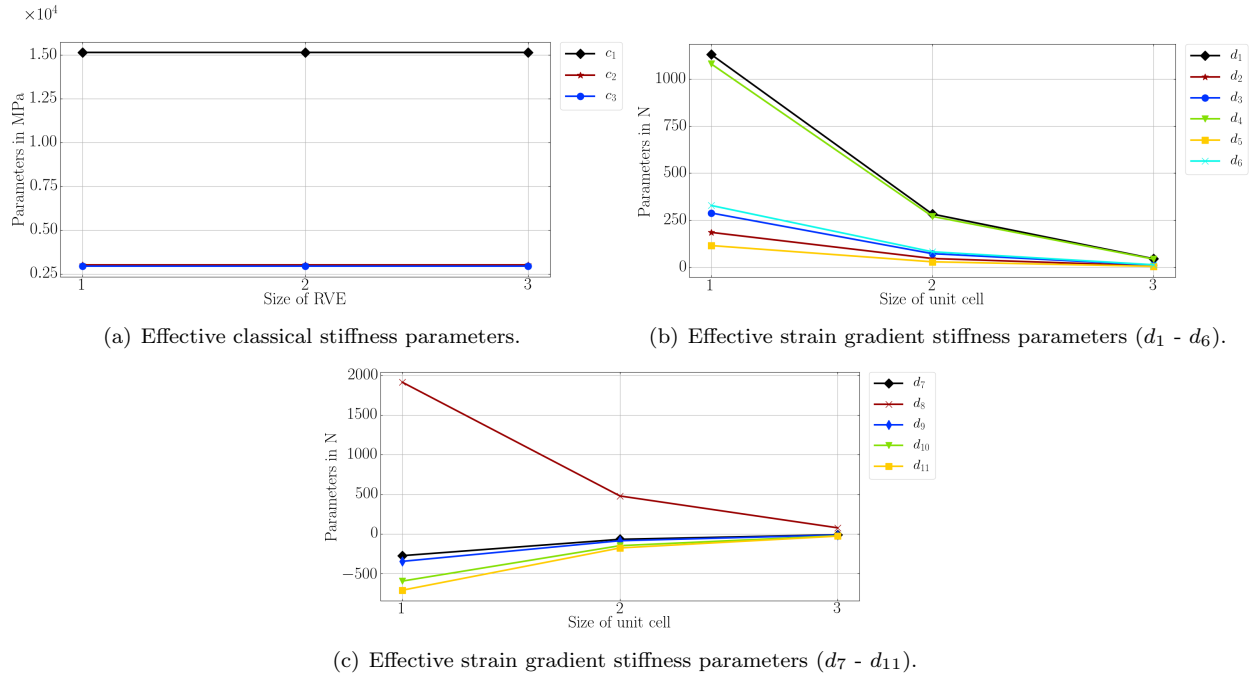


Figure 25: Effective material parameters with changing lengths of unit cells.

5 Remark on positive definiteness

As observed from the previous sections, negative values appear in strain gradient stiffness tensors. This fact may raise concerns regarding the positive definiteness of the strain energy function. In [57, 21, 63, 30], the issue of positive definiteness of the strain energy function for strain gradient materials is addressed and bounds on material parameters are provided. The bounds on strain gradient constants consider the continuum to be purely local, which means that the strain energy function is convex with respect to every material point [57]. However, when homogenizing the microstructures of composite materials with an equivalent strain gradient continuum, we have a limited non-locality. The non-locality originates from the energy equivalence as shown in Eqn. (1). We emphasize that the ϵ is a finite number, $\epsilon < 1$ but not necessarily $\epsilon \ll 1$, which means that the studied composite material has a finite macroscopic and microscopic sizes. Therefore, the strain energy function averaged over this microstructure size should be positive definite and not the pointwise local strain

energy function. Thus coefficients in the strain gradient stiffness tensor could be negative as long as the strain energy density function integrated over the periodic unit cell is positive definite. This interpretation is aligned with in [50, 14, 53].

6 Conclusions

Asymptotic homogenization method was employed to homogenize composite material into effective homogeneous strain gradient continua. Main conclusions are summarized as follows:

- Purely computational analysis determines all the parameters in the strain gradient theory. In particular, the parameters in the rank five tensor and the rank six tensor.
- Numerical examples for 2D and 3D, stiff and soft inclusions, cubic and transverse material symmetry cases were conducted.
- In both 2D and 3D numerical examples, the effective strain gradient parameters vanish when materials are purely homogeneous, they are independent of repetitions of RVEs and sensitive to microstructural sizes.
- Without assuming a specific symmetry group, in the case of cubic symmetry, all expected relations have been captured by the proposed formalism.
- Physical meaning of the homothetic ratio ϵ is interpreted, a so-called scaling rule for effective strain gradient parameters has been discussed. The method is valid when ϵ is a finite value. $\epsilon < 1$ is required but not necessarily $\epsilon \ll 1$.

The homogenization tool is applicable to any composite materials with a periodic substructure at the microscale. Such multiscale are nowadays possible to manufacture by 3D printers. Therefore, effective parameters determination is of interest for a possible topology optimization. Further investigations will focus on the following aspects:

- To validate the identified parameters not only in statics [75] but also in vibration responses, buckling critical loads [47], and wave propagation [69, 31].
- To apply the homogenization method to the analysis of 3D composite materials with finite thickness. This may be achieved by modeling the full thickness unit cell model and relieving the out-of-plane periodicity of the unit cell [62].
- To explore the possibility of studying more sophisticated metamaterials such as the so-called pantographic structures [23, 22, 38, 15] or the biomimetic spinodoids metamaterials [64, 51] by the homogenization method.
- To extend the homogenization method to non-linear regime [35, 27, 33] and multiphysics fields [12, 56, 29].

References

- [1] B. E. Abali. *Computational Reality*, volume 55 of *Advanced Structured Materials*. Springer Nature, Singapore, 2017.
- [2] Bilen Emek Abali and Emilio Barchiesi. Additive manufacturing introduced substructure and computational determination of metamaterials parameters by means of the asymptotic homogenization. *Continuum Mechanics and Thermodynamics*, pages 1–17, 2020.
- [3] Houssam Abdoul-Anziz and Pierre Seppecher. Strain gradient and generalized continua obtained by homogenizing frame lattices. *Mathematics and mechanics of complex systems*, 6(3):213–250, 2018.
- [4] Houssam Abdoul-Anziz, Pierre Seppecher, and Cédric Bellis. Homogenization of frame lattices leading to second gradient models coupling classical strain and strain-gradient terms. *Mathematics and Mechanics of Solids*, 24(12):3976–3999, 2019.

- [5] A Aghaei, N Bochud, G Rosi, and S Naili.
Assessing the effective elastic properties of the tendon-to-bone insertion: a multiscale modeling approach.
Biomechanics and Modeling in Mechanobiology, 20(2):433–448, 2021.
- [6] Jean-Jacques Alibert and Alessandro Della Corte.
Homogenization of nonlinear inextensible pantographic structures by γ -convergence.
Mathematics and Mechanics of Complex Systems, 7(1):1–24, 2019.
- [7] Holm Altenbach and Samuel Forest.
Generalized continua as models for classical and advanced materials.
Springer, 2016.
- [8] Sajad Arabnejad and Damiano Pasini.
Mechanical properties of lattice materials via asymptotic homogenization and comparison with alternative homogenization methods.
International Journal of Mechanical Sciences, 77:249–262, 2013.
- [9] Nicolas Auffray, Regis Bouchet, and Yves Brechet.
Derivation of anisotropic matrix for bi-dimensional strain-gradient elasticity behavior.
International Journal of Solids and Structures, 46(2):440–454, 2009.
- [10] Nicolas Auffray, Justin Dirrenberger, and Giuseppe Rosi.
A complete description of bi-dimensional anisotropic strain-gradient elasticity.
International Journal of Solids and Structures, 69:195–206, 2015.
- [11] Nicolas Auffray, Hung Le Quang, and Qi-Chang He.
Matrix representations for 3D strain-gradient elasticity.
Journal of the Mechanics and Physics of Solids, 61(5):1202–1223, 2013.
- [12] Jean-Louis Auriault, Claude Boutin, and Christian Geindreau.
Homogenization of coupled phenomena in heterogeneous media, volume 149.
John Wiley & Sons, 2010.
- [13] Andrea Bacigalupo, Marco Paggi, F Dal Corso, and D Bigoni.
Identification of higher-order continua equivalent to a Cauchy elastic composite.
Mechanics Research Communications, 93:11–22, 2018.
- [14] Salma Barboura and Jia Li.
Establishment of strain gradient constitutive relations by using asymptotic analysis and the finite element method for complex periodic microstructures.
International Journal of Solids and Structures, 136:60–76, 2018.
- [15] Emilio Barchiesi, Francesco dell’Isola, and François Hild.
On the validation of homogenized modeling for bi-pantographic metamaterials via digital image correlation.
International Journal of Solids and Structures, 208:49–62, 2021.
- [16] Jeremy Bleyer.
Numerical Tours of Computational Mechanics with FEniCS, 2018.
- [17] Helmut J Böhm, Anton Eckschlager, and W Han.
Multi-inclusion unit cell models for metal matrix composites with randomly oriented discontinuous reinforcements.
Computational materials science, 25(1-2):42–53, 2002.
- [18] Claude Boutin.
Microstructural effects in elastic composites.
International Journal of Solids and Structures, 33(7):1023–1051, 1996.
- [19] Claude Boutin, Francesco dell’Isola, Ivan Giorgio, and Luca Placidi.
Linear pantographic sheets: Asymptotic micro-macro models identification.
Mathematics and Mechanics of Complex Systems, 5(2):127–162, 2017.
- [20] Qiang Chen, George Chatzigeorgiou, and Fodil Meraghni.
Extended mean-field homogenization of viscoelastic-viscoplastic polymer composites undergoing hybrid progressive degradation induced by interface debonding and matrix ductile damage.
International Journal of Solids and Structures, 210:1–17, 2020.
- [21] Francesco dell’Isola, Giulio Sciarra, and Stefano Vidoli.
Generalized Hooke’s law for isotropic second gradient materials.

Proceedings of the Royal Society A: Mathematical, Physical and Engineering Sciences, 465(2107):2177–2196, 2009.

- [22] Francesco dell’Isola, Pierre Seppecher, Jean Jacques Alibert, Tomasz Lekszycki, Roman Grygoruk, Marek Pawlikowski, David Steigmann, Ivan Giorgio, Ugo Andreaus, Emilio Turco, Maciej Gołaszewski, Nicola Rizzi, Claude Boutin, Victor A. Eremeyev, Anil Misra, Luca Placidi, Emilio Barchiesi, Leopoldo Greco, Massimo Cuomo, Antonio Cazzani, Alessandro Della Corte, Antonio Battista, Daria Scerrato, Inna Zurba Eremeeva, Yosra Rahali, Jean-François Ganghoffer, Wolfgang Müller, Gregor Ganzosch, Mario Spagnuolo, Aron Pfaff, Katarzyna Barcz, Klaus Hoschke, Jan Negggers, and François Hild. Pantographic metamaterials: an example of mathematically driven design and of its technological challenges. *Continuum Mechanics and Thermodynamics*, 31(4):851–884, 2019.
- [23] Francesco dell’Isola, Pierre Seppecher, Mario Spagnuolo, Emilio Barchiesi, François Hild, Tomasz Lekszycki, Ivan Giorgio, Luca Placidi, Ugo Andreaus, Massimo Cuomo, Simon R. Eugster, Aron Pfaff, Klaus Hoschke, Ralph Langkemper, Emilio Turco, Rizacan Sarikaya, Aviral Misra, Michele De Angelo, Francesco D’Annibale, Amine Bouterf, Xavier Pinelli, Anil Misra, Boris Desmorat, Marek Pawlikowski, Corinne Dupuy, Daria Scerrato, Patrice Peyre, Marco Laudato, Luca Manzari, Peter Göransson, Christian Hesch, Sofia Hesch, Patrick Franciosi, Justin Dirrenberger, Florian Maurin, Zacharias Vangelatos, Costas Grigoropoulos, Vasileia Melissinaki, Maria Farsari, Wolfgang Müller, Bilen Emek Abali, Christian Liebold, Gregor Ganzosch, Philip Harrison, Rafał Drobnicki, Leonid Igumnov, Faris Alzahrani, and Tasawar Hayat. Advances in pantographic structures: design, manufacturing, models, experiments and image analyses. *Continuum Mechanics and Thermodynamics*, 31(4):1231–1282, 2019.
- [24] Justin Dirrenberger, Samuel Forest, and Dominique Jeulin. Computational homogenization of architected materials. In Yuri Estrin, Yves Bréchet, John Dunlop, and Peter” Fratzl, editors, *Architected materials in nature and engineering*, Springer Series in Materials Science, pages 89–139. Springer, 2019.
- [25] F Dos Reis and JF Ganghoffer. Construction of micropolar continua from the asymptotic homogenization of beam lattices. *Computers & Structures*, 112:354–363, 2012.
- [26] F Dos Reis and JF Ganghoffer. Equivalent mechanical properties of auxetic lattices from discrete homogenization. *Computational Materials Science*, 51(1):314–321, 2012.
- [27] Khaled ElNady, Ibrahim Goda, and Jean-François Ganghoffer. Computation of the effective nonlinear mechanical response of lattice materials considering geometrical nonlinearities. *Computational Mechanics*, 58(6):957–979, 2016.
- [28] Victor A Eremeyev. On effective properties of materials at the nano-and microscales considering surface effects. *Acta Mechanica*, 227(1):29–42, 2016.
- [29] Victor A Eremeyev, Jean-François Ganghoffer, Violetta Konopińska-Zmysłowska, and Nikolay S Uglov. Flexoelectricity and apparent piezoelectricity of a pantographic micro-bar. *International Journal of Engineering Science*, 149:103213, 2020.
- [30] Victor A Eremeyev, Sergey A Lurie, Yury O Solyaev, and Francesco dell’Isola. On the well posedness of static boundary value problem within the linear dilatational strain gradient elasticity. *Zeitschrift für angewandte Mathematik und Physik*, 71(6):1–16, 2020.
- [31] Victor A Eremeyev, Giuseppe Rosi, and Salah Naili. Comparison of anti-plane surface waves in strain-gradient materials and materials with surface stresses. *Mathematics and mechanics of solids*, 24(8):2526–2535, 2019.
- [32] A Cemal Eringen. Theory of micropolar elasticity. In *Microcontinuum field theories*, pages 101–248. Springer, 1999.
- [33] Jacob Fish, Zhiqiang Yang, and Zifeng Yuan. A second-order reduced asymptotic homogenization approach for nonlinear periodic heterogeneous materials.

- International Journal for Numerical Methods in Engineering*, 119(6):469–489, 2019.
- [34] Samuel Forest.
Micromorphic media.
In *Generalized continua from the theory to engineering applications*, pages 249–300. Springer, 2013.
- [35] Samuel Forest.
Continuum thermomechanics of nonlinear micromorphic, strain and stress gradient media.
Philosophical Transactions of the Royal Society A, 378(2170):20190169, 2020.
- [36] Samuel Forest and Duy Khanh Trinh.
Generalized continua and non-homogeneous boundary conditions in homogenisation methods.
ZAMM-Journal of Applied Mathematics and Mechanics/Zeitschrift für Angewandte Mathematik und Mechanik, 91(2):90–109, 2011.
- [37] JF Ganghoffer and H Reda.
A variational approach of homogenization of heterogeneous materials towards second gradient continua.
Mechanics of Materials, page 103743, 2021.
- [38] Ivan Giorgio, Valerio Varano, Francesco dell’Isola, and Nicola L Rizzi.
Two layers pantographs: a 2D continuum model accounting for the beams’ offset and relative rotations as averages in SO (3) lie groups.
International Journal of Solids and Structures, 2021.
- [39] Ibrahim Goda, Mohamed Assidi, and Jean-François Ganghoffer.
Equivalent mechanical properties of textile monolayers from discrete asymptotic homogenization.
Journal of the Mechanics and Physics of Solids, 61(12):2537–2565, 2013.
- [40] Ibrahim Goda and Jean-François Ganghoffer.
Construction of first and second order grade anisotropic continuum media for 3d porous and textile composite structures.
Composite Structures, 141:292–327, 2016.
- [41] Stefano Gonella and Massimo Ruzzene.
Homogenization and equivalent in-plane properties of two-dimensional periodic lattices.
International Journal of Solids and Structures, 45(10):2897–2915, 2008.
- [42] Behrooz Hassani and Ernest Hinton.
A review of homogenization and topology optimization I—homogenization theory for media with periodic structure.
Computers & Structures, 69(6):707–717, 1998.
- [43] Scott J Hollister and Noboru Kikuchi.
A comparison of homogenization and standard mechanics analyses for periodic porous composites.
Computational mechanics, 10(2):73–95, 1992.
- [44] Geralf Hütter.
Homogenization of a Cauchy continuum towards a micromorphic continuum.
Journal of the Mechanics and Physics of Solids, 99:394–408, 2017.
- [45] Lukáš Jakabčín and Pierre Seppecher.
On periodic homogenization of highly contrasted elastic structures.
Journal of the Mechanics and Physics of Solids, 144:104104, 2020.
- [46] Toufik Kanit, Samuel Forest, Isabelle Galliet, Valérie Mounoury, and Dominique Jeulin.
Determination of the size of the representative volume element for random composites: statistical and numerical approach.
International Journal of Solids and Structures, 40(13-14):3647–3679, 2003.
- [47] Sergei Khakalo, Viacheslav Balobanov, and Jarkko Niiranen.
Modelling size-dependent bending, buckling and vibrations of 2d triangular lattices by strain gradient elasticity models: applications to sandwich beams and auxetics.
International Journal of Engineering Science, 127:33–52, 2018.
- [48] Varvara Kouznetsova, Marc GD Geers, and WA Marcel Brekelmans.
Multi-scale constitutive modelling of heterogeneous materials with a gradient-enhanced computational homogenization scheme.
International journal for numerical methods in engineering, 54(8):1235–1260, 2002.

- [49] VG Kouznetsova, Marc GD Geers, and WAM1112 Brekelmans.
Multi-scale second-order computational homogenization of multi-phase materials: a nested finite element solution strategy.
Computer methods in applied Mechanics and Engineering, 193(48-51):5525–5550, 2004.
- [50] Rajesh S Kumar and David L McDowell.
Generalized continuum modeling of 2-D periodic cellular solids.
International Journal of solids and structures, 41(26):7399–7422, 2004.
- [51] Siddhant Kumar, Stephanie Tan, Li Zheng, and Dennis M Kochmann.
Inverse-designed spinodoid metamaterials.
npj Computational Materials, 6(1):1–10, 2020.
- [52] Jia Li.
A micromechanics-based strain gradient damage model for fracture prediction of brittle materials—part i: Homogenization methodology and constitutive relations.
International journal of solids and structures, 48(24):3336–3345, 2011.
- [53] Jia Li and Xiao-Bing Zhang.
A numerical approach for the establishment of strain gradient constitutive relations in periodic heterogeneous materials.
European Journal of Mechanics-A/Solids, 41:70–85, 2013.
- [54] Shutian Liu and Wenzheng Su.
Effective couple-stress continuum model of cellular solids and size effects analysis.
International Journal of Solids and Structures, 46(14-15):2787–2799, 2009.
- [55] K. K. Mandadapu, B. E. Abali, and P. Papadopoulos.
On the polar nature and invariance properties of a thermomechanical theory for continuum-on-continuum homogenization.
Mathematics and Mechanics of Solids, pages 1–18, 2021.
- [56] Nagham Mawassy, Hilal Reda, Jean-Francois Ganghoffer, Victor A Eremeyev, and Hassan Lakiss.
A variational approach of homogenization of piezoelectric composites towards piezoelectric and flexoelectric effective media.
International Journal of Engineering Science, 158:103410, 2021.
- [57] Raymond David Mindlin and NN Eshel.
On first strain-gradient theories in linear elasticity.
International Journal of Solids and Structures, 4(1):109–124, 1968.
- [58] Anil Misra and Payam Poorsolhjoui.
Identification of higher-order elastic constants for grain assemblies based upon granular micromechanics.
Mathematics and Mechanics of Complex Systems, 3(3):285–308, 2015.
- [59] Vincent Monchiet, Nicolas Auffray, and Julien Yvonnet.
Strain-gradient homogenization: a bridge between the asymptotic expansion and quadratic boundary condition methods.
Mechanics of Materials, 143:103309, 2020.
- [60] Wolfgang H Müller.
The experimental evidence for higher gradient theories.
In A Bertram and S Forest, editors, *Mechanics of Strain Gradient Materials*, volume 600 of *CISM International Centre for Mechanical Sciences*, pages 1–18. Springer, 2020.
- [61] He Nassar, Q-C He, and Nicolas Auffray.
A generalized theory of elastodynamic homogenization for periodic media.
International Journal of Solids and Structures, 84:139–146, 2016.
- [62] Muhammad Ridlo Erdata Nasution, Naoyuki Watanabe, Atsushi Kondo, and Arief Yudhanto.
A novel asymptotic expansion homogenization analysis for 3-D composite with relieved periodicity in the thickness direction.
Composites science and technology, 97:63–73, 2014.
- [63] Lidiia Nazarenko, Rainer Glüge, and Holm Altenbach.
Positive definiteness in coupled strain gradient elasticity.
Continuum Mechanics and Thermodynamics, pages 1–13, 2020.

- [64] Carlos M Portela, A Vidyasagar, Sebastian Krödel, Tamara Weissenbach, Daryl W Yee, Julia R Greer, and Dennis M Kochmann.
Extreme mechanical resilience of self-assembled nanolabyrinthine materials.
Proceedings of the National Academy of Sciences, 117(11):5686–5693, 2020.
- [65] Y Rahali, I Giorgio, JF Ganghoffer, and F dell’Isola.
Homogenization à la Piola produces second gradient continuum models for linear pantographic lattices.
International Journal of Engineering Science, 97:148–172, 2015.
- [66] Yosra Rahali, VA Eremeyev, and Jean-François Ganghoffer.
Surface effects of network materials based on strain gradient homogenized media.
Mathematics and Mechanics of Solids, 25(2):389–406, 2020.
- [67] Ondřej Rokoš, Maqsood M Ameen, Ron HJ Peerlings, and Mark GD Geers.
Micromorphic computational homogenization for mechanical metamaterials with patterning fluctuation fields.
Journal of the Mechanics and Physics of Solids, 123:119–137, 2019.
- [68] Giuseppe Rosi.
Waves and generalized continua.
In H Altenbach and A Öchsner, editors, *Encyclopedia of Continuum Mechanics*, pages 2756–2765. Springer, 2020.
- [69] Giuseppe Rosi and Nicolas Auffray.
Anisotropic and dispersive wave propagation within strain-gradient framework.
Wave Motion, 63:120–134, 2016.
- [70] Giuseppe Rosi, Luca Placidi, and Nicolas Auffray.
On the validity range of strain-gradient elasticity: a mixed static-dynamic identification procedure.
European Journal of Mechanics-A/Solids, 69:179–191, 2018.
- [71] Andrzej Skrzat and Victor A Eremeyev.
On the effective properties of foams in the framework of the couple stress theory.
Continuum Mechanics and Thermodynamics, pages 1–23, 2020.
- [72] Valery P Smyshlyaev and Kirill D Cherednichenko.
On rigorous derivation of strain gradient effects in the overall behaviour of periodic heterogeneous media.
Journal of the Mechanics and Physics of Solids, 48(6-7):1325–1357, 2000.
- [73] Oliver Weeger.
Numerical homogenization of second gradient, linear elastic constitutive models for cubic 3d beam-lattice metamaterials.
International Journal of Solids and Structures, 2021.
- [74] Hua Yang, Bilen Emek Abali, Dmitry Timofeev, and Wolfgang H Müller.
Determination of metamaterial parameters by means of a homogenization approach based on asymptotic analysis.
Continuum Mechanics and Thermodynamics, pages 1–20, 2019.
- [75] Hua Yang, Dmitry Timofeev, Ivan Giorgio, and Wolfgang H Müller.
Effective strain gradient continuum model of metamaterials and size effects analysis.
Continuum Mechanics and Thermodynamics, pages 1–23, 2020.
- [76] Marcus Yoder, Lonny Thompson, and Joshua Summers.
Size effects in lattice structures and a comparison to micropolar elasticity.
International Journal of Solids and Structures, 143:245–261, 2018.
- [77] Wenbin Yu and Tian Tang.
Variational asymptotic method for unit cell homogenization of periodically heterogeneous materials.
International Journal of Solids and Structures, 44(11-12):3738–3755, 2007.
- [78] J Yvonnet, Nicolas Auffray, and V Monchiet.
Computational second-order homogenization of materials with effective anisotropic strain-gradient behavior.
International Journal of Solids and Structures, 191:434–448, 2020.